TRƯỜNG ĐẠI HỌC QUY NHƠN
QUY NHON UNIVERSITY

TẠP CHÍ KHOA HỌC
TRƯỜNG ĐẠI HỌC QUY NHƠN

QUY NHON UNIVERSITY
JOURNAL OF SCIENCE

KHOA HỌC TỰ NHIÊN VÀ KỸ THUẬT
NATURAL SCIENCES AND ENGINEERING

18 (3)

2024

JUNE 2024

QUY NHON UNIVERSITY
JOURNAL OF SCIENCE
VOLUME 18, ISSUE 3, JUNE 2024
ISSN: 1859-0357 E-ISSN: 2815-6242

CONTENTS

TẠP CHÍ KHOA HỌC
TRƯỜNG ĐẠI HỌC QUY NHƠN

Nghiên cứu sự trao đổi và hấp phụ các cation kim loại trên bề mặt kaolinite từ lý thuyết phiếm hàm mật độ

Nguyễn Ngọc Trí*, Nguyễn Thị Lan

Phòng thí nghiệm Hóa học tính toán và Mô phỏng (LCCM), Khoa Khoa học Tự nhiên, Trường Đại học Quy Nhơn, Việt Nam

Ngày nhận bài: 03/10/2023; Ngày sửa bài: 10/01/2024;
Ngày nhận đăng: 22/01/2024; Ngày xuất bản: 28/06/2024

TÓM TẮT

Trong nghiên cứu này các quá trình trao đổi và hấp phụ các cation kim loại được khảo sát sử dụng các tính toán theo các nguyên lý đầu tiên. Các kết quả thu được chỉ ra rằng, các sự trao đổi cation hầu như không thuận lợi, trong đó các vị trí Al^{3+} dễ thay thế hơn Si^{4+}. Các cation kim loại được hấp phụ mạnh mẽ trên kaolinite ở cả hai mặt H-slab và O-slab. Kết quả tính tại phiếm hàm PBE, khả năng hấp phụ các cation kim loại giảm theo thứ tự $Li^+ > K^+ > Na^+ > Ca^{2+} > Al^{3+} > Fe^{3+} > Cr^{3+} > Mg^{2+}$. Đáng chú ý, sự xâm nhập vào cấu trúc tinh thể của kaolinite được phát hiện đối với Li^+ và Mg^{2+} ở mặt H-slab cùng với sự hình thành tương ứng các liên kết mới Li-O và Mg-O. Trong khi đó, sự xen vào giữa các lớp kaolinite bởi các cation Ca^{2+} được phát hiện với sự hình thành các liên kết Ca-O với cả hai mặt H-slab và O-slab. Đối với Na^+, K^+, hay Cr^{3+}, sự ưu tiên ở bề mặt O-slab trong quá trình hấp phụ. Trong khi đó, Al^{3+} và Fe^{3+} tạo sự tương tác tốt ở trên bề mặt H-slab. Các phân tích mật độ trạng thái và phân bố mật độ electron chứng tỏ sự hình thành các liên kết cộng hóa trị M-O trong quá trình hấp phụ. Hơn nữa, K^+ được đề xuất như là sự bổ sung trên bề mặt kaolinite đối với các khảo sát xa hơn về hấp phụ và loại bỏ hiệu quả các hợp chất hữu cơ trong các môi trường.

Từ khóa: *Sự trao đổi, hấp phụ, cation kim loại, kaolinite, DFT.*

**Tác giả liên hệ chính.*
Email: nguyenngoctri@qnu.edu.vn

QUY NHON UNIVERSITY
JOURNAL OF SCIENCE

Metal cation exchange and adsorption onto kaolinite surfaces: a DFT study

Nguyen Ngoc Tri*, Nguyen Thi Lan

Laboratory of Computational Chemistry and Modelling (LCCM), Faculty of Natural Sciences, Quy Nhon University, Vietnam

Received: 03/10/2023; Revised: 10/01/2024; Accepted: 22/01/2024; Published: 28/06/2024

ABSTRACT

In this study, metal cations exchange and adsorption processes onto kaolinite surfaces are investigated using first-principles calculations. Obtained results indicate that the exchanges of cations are mostly unfavorable, and the Al sites are conveniently replaced compared to Si sites. The metal cations are adsorbed strongly onto kaolinite surfaces at both O-slab and H-slab. The adsorption ability of metal cations decreases in the order of $Li^+ > K^+ > Na^+ > Ca^{2+} > Al^{3+} > Fe^{3+} > Cr^{3+} > Mg^{2+}$ at the PBE functional. Remarkably, the insertions of Li^+ and Mg^{2+} into the lattice structure of kaolinite are found at H-slab following the formation of Li-O and Mg-O new bonds, respectively. The intercalation into kaolinite by Ca^{2+} is observed in forming Ca-O bonds for both H-slab and O-slab. For Na^+, K^+, and Cr^{3+}, the favorable attachment is located at the O-slab upon adsorption. Besides, the Al^{3+} and Fe^{3+} ions interact preferably on the H-slab. The analyses of the density of states and electron localization function clarify the appearance of M-O covalent bonds upon the adsorption process. Further, K^+ is suggested as a promising addition to kaolinite surfaces for the efficient adsorption and removal of organic compounds in environments.

Keywords: *Exchange, adsorption, metal cations, kaolinite, DFT.*

1. INTRODUCTION

Kaolinite is one of two-layer aluminosilicates, containing the hydrogen-rich surface (H-slab) and oxygen-rich surface (O-slab). The H-slab with high positive charge density is favorable for interaction with organic compounds containing functional groups such as -OH, -COOH.[1-3] In particular, the adsorptions of benzene, n-hexane, pyridine, and 2-propanol on H-slab are more substantial than those on O-slab.[4] Similarly, phenol, toluene, and CO_2 are adsorbed preferably on the kaolinite aluminol surface (H-slab).[5] In contrast, the O-slab containing a sizeable negative charge density is considered an efficient surface for the adhesion of metal cations or other cations.[6-8] As a result, kaolinite is one of the potential materials for the adsorption and removal of heavy metals from aquatic environments.[9] Besides, theoretical approaches using density functional theory (DFT) provide insight into the adsorption process of metal cations on material surfaces.[1-8]

It is noticeable that the exchange of cations in the material structure leads to considerable changes in electronic and surface properties, increasing the applicability of materials, especially in energy and environment fields.[10] Recently, the alkali activated kaolinite

*Corresponding author.
Email: nguyenngoctri@qnu.edu.vn

https://doi.org/10.52111/qnjs.2024.18301

has been investigated for antibiotic adsorption.[11] Accordingly, replacing Al^{3+}/Si^{4+} on kaolinite with Na^{+} cations improves adsorption performance. In another report, the hydrated form of Cd(II) adsorbed on basal planes of kaolinite (H-slab and O-slab) was carried out using theoretical approach.[12] Moreover, Cs(I) adsorption on kaolinite was more convenient for O-slab than for H-slab.[13] It can be seen that the hydrated forms of metal cations and material surfaces in aquatic environments are quite complex, affected by various factors such as temperature, pressure, concentration, pH, and the presence of other compounds. Additionally, the suitable planar surface of kaolinite for the cation adsorption was not clarified in the previous studies. Therefore, in the present work, we use DFT calculations to investigate the replacement of exchangeable cations in the structure of kaolinite (Al^{3+}, Si^{4+}), and adsorption of various cations with the unhydrated form on both H-slab and O-slab, to have an insight into the structural and electronic properties, surface interactions. Furthermore, results are expected to suggest promising metal cations adding to the kaolinite surface for the good adsorption and removal of organic pollutants in environments.

2. COMPUTATIONAL METHOD

The geometric structures of the kaolinite surfaces and adsorption configurations are optimized by VASP.[14] Kaolinite is one of the common clay minerals, including a series of uncharged layers connected by a network of hydrogen bonds between H-slab and O-slab, as shown in Figure 1. In this work, the *1 x 1 x 1* (for one layer in exchange) and *2 x 1 x 1* (for two layers in adsorption) cell models are designed with dimensions size of the unit cell in experiments[15]: a = 5.15 Å; b = 8.93 Å; c = 7.38 Å, and a = 10.30 Å; b = 8.93 Å; c = 28.51 Å, respectively. The vacuum space in the two-layered structure is 15 Å, large enough to ignore boundary interactions between two slabs. Plane-wave cutoff energy is set up at 500 eV upon optimization.

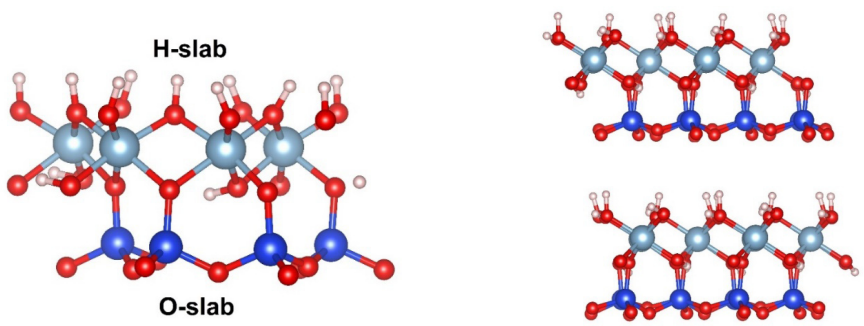

Figure 1. The surface models of kaolinite in this work.

In addition, the Perdew-Burke-Ernzerhof (PBE) function with a generalized gradient approximation (GGA) for the exchange-correlation component is used in all calculations.[16] Adsorption energy (E_{ads}) is computed by using the following expressions:

$$E_{ads} = E_{comp} - E_{kaoli} - E_{M}$$

where E_{comp}, E_{kaoli} and E_{M} are the energy values of complexes, kaolinite surfaces, and metal cations, respectively. The exchange energy (E_{exh}) of metal cations into the lattice structure of kaolinite is determined as follows:

$$E_{exh} = E_{kaoli\text{-}M} + E_{Al/Si} - E_{M} - E_{kaoli}$$

in which $E_{kaoli\text{-}M}$ and $E_{Al/Si}$ correspond to the energy values of the new structure of cation exchange and Al^{3+}/Si^{4+}. Moreover, to understand the formation of stable structures, the density of states (DOS) and electronic localization function (ELF) analyses are carried out at the same level of theory.

3. RESULTS AND DISCUSSION

3.1. Optimized structures

The stable configurations of exchange and adsorption of metal cations (M), including Li^+, Na^+, K^+, Mg^{2+}, Ca^{2+}, Al^{3+}, $Cr^{3+,}$ and Fe^{3+} based on DFT calculations at PBE functional, are presented in Figures 2 and 3. Accordingly, the cation exchange occurs at Al^{3+} or Si^{4+} sites of kaolinite lattice structure. Some Al-O or Si-O bonds are broken and replaced by new M-O bonds upon optimization. The bond lengths of Al/Si-O in kaolinite are ca. 1.85-2.00 Å (Al) and 1.61-1.64 Å (Si), consistent with experiment values in previous studies.[17]

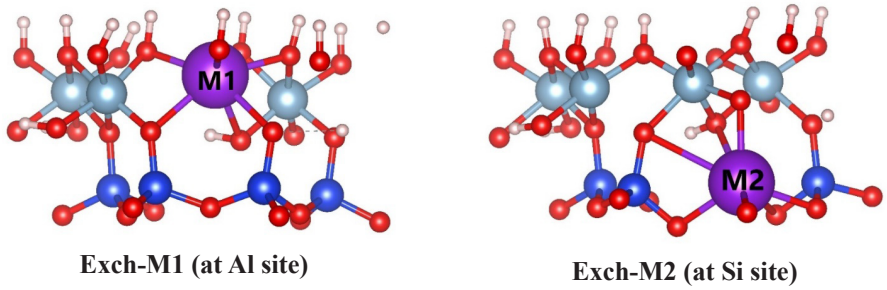

Figure 2. The optimized structures of cations exchange on kaolinite surfaces.

For derivatives in exchange, the M-O bond lengths for replacement of Al^{3+} (denoted by M1) and Si^{4+} (denoted by M2) sites are 1.97-2.24 Å (Li1), 1.80-1.89 Å (Li2), 2.13-2.37 Å (Na1), 2.08-2.17 Å (Na2), 2.35-2.89 Å (K1), 2.30-3.15 Å (K2), 1.99-2.07 Å (Mg1), 1.86-1.92 Å (Mg2), 2.18-2.30 Å (Ca1), 2.11-2.73 Å (Ca2), 1.73-1.75 Å (Al2), 1.84-1.99 Å (Si1), 1.91-2.03 Å (Cr1), 1.72-1.80 Å (Cr2), 1.88-2.01 Å (Fe1), 1.73-1.81 Å (Fe2). As a result, the M-O distances are larger at M2 than at M1 structures following the cation exchange. Moreover, the charge densities surrounding Al/Si sites in kaolinite change in replacing metal cations. Hence, the cation substitutions lead to considerable changes in M-O bond length and charge density on M, which could cause a decrease in structure strength compared to original kaolinite.

In addition, the adsorption of metal cations onto kaolinite is observed at the H-slab, O-slab, and between two of these slabs, as displayed in Figure 3. According to the optimization, metal cations attach on H-slab at the O sites to form M-O interactions in **Ads-M1**, while the adhesion of metal cations on O-slab is preferred at the tetragonal cage in **Ads-M3** and hexagonal cage in **Ads-M4**. The attachment of cations into the interlayer of H-slab and O-slab is considered in the present work. Here, the configurations are stabilized by M-O new bonds in **Ads-M2**.

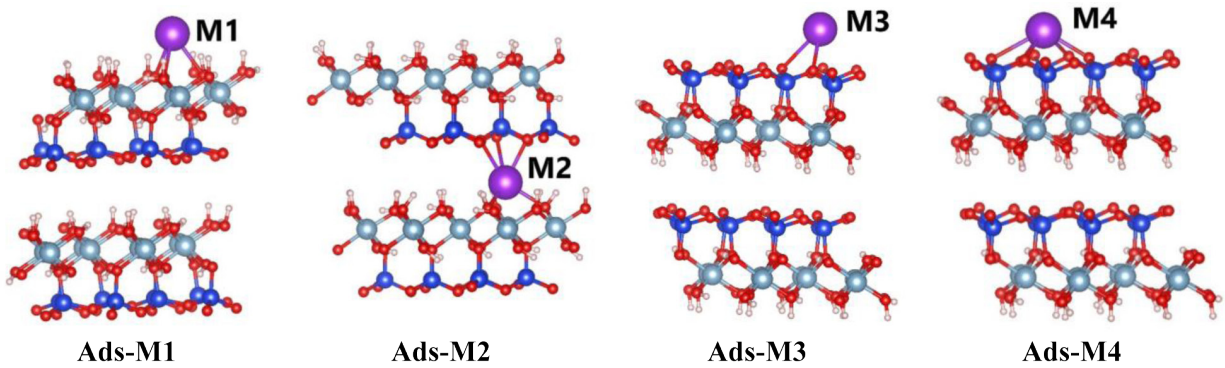

Figure 3. The stable structures of cations adsorption on kaolinite surfaces.

https://doi.org/10.52111/qnjs.2024.18301

The interaction distances in adsorption configurations (**Ads-M1**, **Ads-M2**, **Ads-M3**, **Ads-M4**) are mostly larger than M-O bond lengths in cation exchange. In particular, the M-O distances are ca. 2.66-2.69 Å (Li1), 2.04-2.29 Å (Li2), 1.90-2.57 Å (Li3), 2.08-2.50 Å (Li4), 2.45-2.50 Å (Na1), 2.27-2.90 Å (Na2), 2.35-2.66 Å (Na3), 2.39-2.95 Å (Na4), 2.80-2.82 Å (K1), 2.49-3.02 Å (K2), 2.65-3.06 Å (K3), 2.75-3.14 Å (K4), 2.22 Å (Mg1), 2.05-2.14 Å (Mg2), 2.92 Å (Mg3), 3.25 Å (Mg4), 2.42 Å (Ca1), 2.32-2.73 Å (Ca2), 2.40 Å (Ca3), 2.47-2.50 Å (Ca4), 2.01 Å (Al1), 2.14-3.08 Å (Al2), 2.16 Å (Al3), 2.31-2.94 Å (Al4), 2.50-2.65 Å (Cr1), 2.13-3.02 Å (Cr2), 2.27 Å (Cr3), 2.28 Å (Cr4), 2.38-2.69 Å (Fe1), 1.97-3.56 Å (Fe2), 2.23 Å (Fe3), 2.45-2.92 Å (Fe4) upon adsorptions. Noticeably, the Li^+ and Mg^{2+} cations tend to insert into the lattice structure of kaolinite and form Li-O and Mg-O new bonds along with Al-O bonds at H-slab.

3.2. Exchange and adsorption energies

The characteristic parameters such as the exchange energy (E_{exh}) and adsorption energy (E_{ads}) calculated and gathered in Table 1 aim to evaluate the exchange and adsorption ability of cations onto kaolinite surfaces.

Table 1. The energy of cation exchange (E_{exh}) and adsorption (E_{ads}) on kaolinite (in kcal.mol^{-1}).

	M	Li^+	Na^+	K^+	Mg^{2+}	Ca^{2+}	Al^{3+}	Cr^{3+}	Fe^{3+}
E_{exh}	**Exch-M1**	214.7	250.0	282.5	126.1	123.2	--	**57.7**	96.6
	Exch-M2	284.5	326.5	357.6	210.9	210.6	**70.9**	92.3	132.8
E_{ads}	**Ads-M1**	-12.9	-12.1	-12.7	-5.5	-11.8	**-22.6**	-6.7	**-11.7**
	Ads-M2	**-61.9**	-25.9	-14.6	**-7.0**	**-24.3**	-12.0	-6.7	-10.5
	Ads-M3	-26.8	-21.4	-25.3	-0.7	-14.2	-18.1	-7.9	-8.1
	Ads-M4	-42.1	**-29.8**	**-33.5**	-0.8	-21.6	-17.4	**-8.7**	-7.1

Calculated results show that the exchange energy values are highly positive, in the range of 57.7 - 357.6 kcal.mol^{-1}, indicating these processes are endothermic and thermodynamically unfavorable. This result is consistent with the previous report on substitutions in kaolinite by combining ions from groups II and III.[18] As a result, the replacement of Al^{3+}/Si^{4+} with Cr^{3+}, and Fe^{3+} are more convenient than other cations. The cation exchanges are more favorable at the Al^{3+} than at Si^{4+}, especially the Cr-derivative (E_{exh} ca. 57.7 kcal.mol^{-1}). With the Si^{4+} substitutions, the Al-derivative (E_{exh} ca. 70.9 kcal.mol^{-1}) is formed more preferably than other ones. Here, it can be understood that the changes in charge density and radius of the metal cations yield changes in geometrical structures. The substituted metal cations mostly have a smaller charge and a much different radius than the substituted Al^{3+}/Si^{4+} in kaolinite, leading to the formation of less stable structures.

Considering the adsorption of metal cations onto H-slab and O-slab, the adsorption energy (E_{ads}) ranges from -7.0 to -61.9 kcal. mol^{-1}. The obtained configurations are thus relatively stable. The metal cations are adsorbed strongly to different sites onto kaolinite surfaces. Specifically, Li^+ cations tend to insert into the kaolinite in the octahedral cage and form Li-O new bonds in the **Ads-Li2** (E_{ads} = -61.9 kcal. mol^{-1}), the most stable structure in investigated systems. The **Ads-Li4** is formed conveniently with an adsorption energy value of -42.1 kcal. mol^{-1}, and Li-O bonds located at the octahedral cage of the O-slab. This is due to the Li^+ ion has the smallest radius among the investigated cations, so it is conveniently located at cages of H-slab and O-slab and inserted into the lattice structure of kaolinite. Besides, Na^+, K^+, and Cr^{3+} cations interact considerably with O sites on the O-slab in forming the **Ads-Na4**, **Ads-K4,** and **Ads-Cr4** with corresponding adsorption energies of -29.8,

-33.5, and -8.7 kcal.mol^{-1}. These structures are much more stable than **Ads-Na1**, **Ads-K1**, and **Ads-Cr1** where the adsorption occurs preferably on the H-slab.

In addition, the Al^{3+} and Fe^{3+} cations are adsorbed strongly at the H-slab leading to the existence of M-O bonds at the top of the tetrahedral cage in **Ads-Al1** (E_{ads} of - 22.6 kcal.mol^{-1}) and **Ads-Fe1** (E_{ads} of -11.7 kcal.mol^{-1}). These configurations are about 4-5 kcal.mol^{-1}, more stable than **Ads-Al4** and **Ads-Fe4**. With the remaining metal cations (Mg^{2+}, Ca^{2+}), the most stable configurations are **Ads-Mg2** and **Ads-Ca2** with the intercalation of ions between the H-slab and O-slab. Here, Mg^{2+} inserts into the H-slab and forms Mg-O bonds similar to Li^{+}. However, the **Ads-Mg2** (E_{ads} of -7.0 kcal.mol^{-1}) is much less stable than **Ads-Li2**. Meanwhile, the intercalation of Ca^{2+} yields the appearance of Ca-O bonds with both H-slab and O-slab. The **Ads-Ca2** is thus relatively stable in this case, with an adsorption energy of -24.3 kcal.mol^{-1}. Furthermore, results indicate that among the common metal cations in aqueous environments (Na^{+}, K^{+}, Mg^{2+}, and Ca^{2+}), K^{+} has the best adsorption ability on kaolinite surfaces. In previous reports, the alkali metal (Na, Mg, Ca) supported on kaolinite enhances the adsorption capacity of heavy metal.[19,20] From this aspect, K^{+} is expected to be a good candidate to support kaolinite surfaces for the adsorption of heavy metals and organic compounds.

3.3. DOS and ELF analyses

To better understand the formation of structures following the exchange and adsorption of cations, the density of states (DOS) and electron localization function (ELF) analyses at the PBE function are examined and illustrated in Figures 4 and 5.

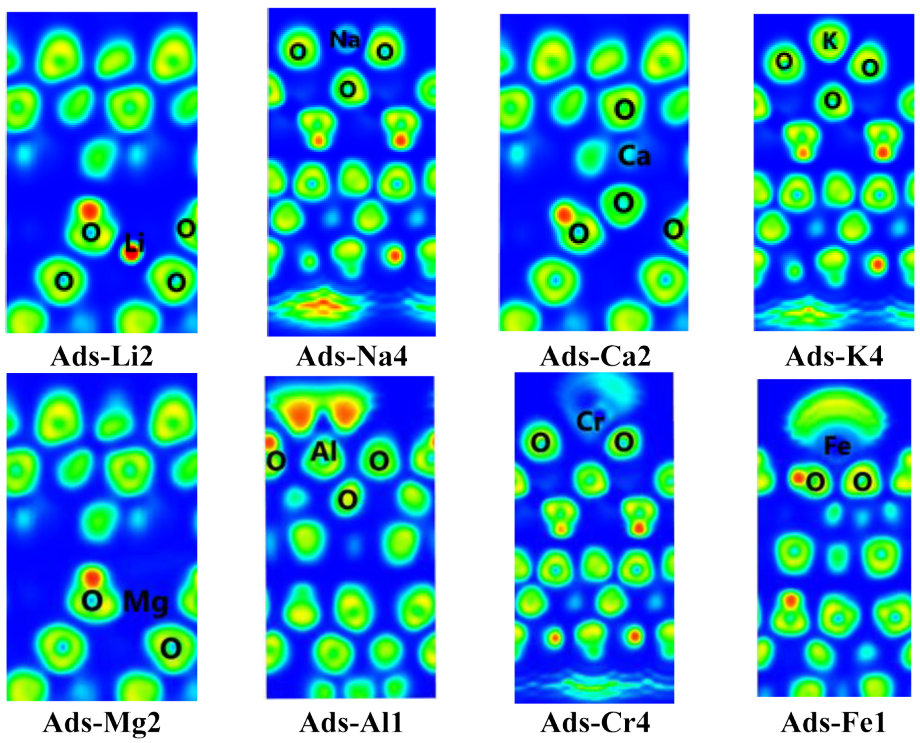

Figure 4. The ELF maps of the most stable adsorption configurations.

Results of ELF analysis indicate that the interactions are formed between M metals and O at the H-slab and O-slab with highly localized electron density, regarded as the chemical bonds.[21] The electron density sharing between M-O bonds is more favorable at the O-slab surface than at the H-slab. Moreover, the electron density localized at the M-O bonds for

https://doi.org/10.52111/qnjs.2024.18301

the structures is considerably high and decreases from **Ads-Li2**, **Ads-K4**, and **Ads-Na4**, going to **Ads-Ca2**, **Ads-Al1**, and finally in **Ads -Fe1**, **Ads-Cr4**, **Ads-Mg2**. Therefore, the formation of M-O covalent bonds is preferred in the order of Li, K, Na > Ca, Al > Fe, Cr, and Mg, consistent with the difference in adsorption energy values above.

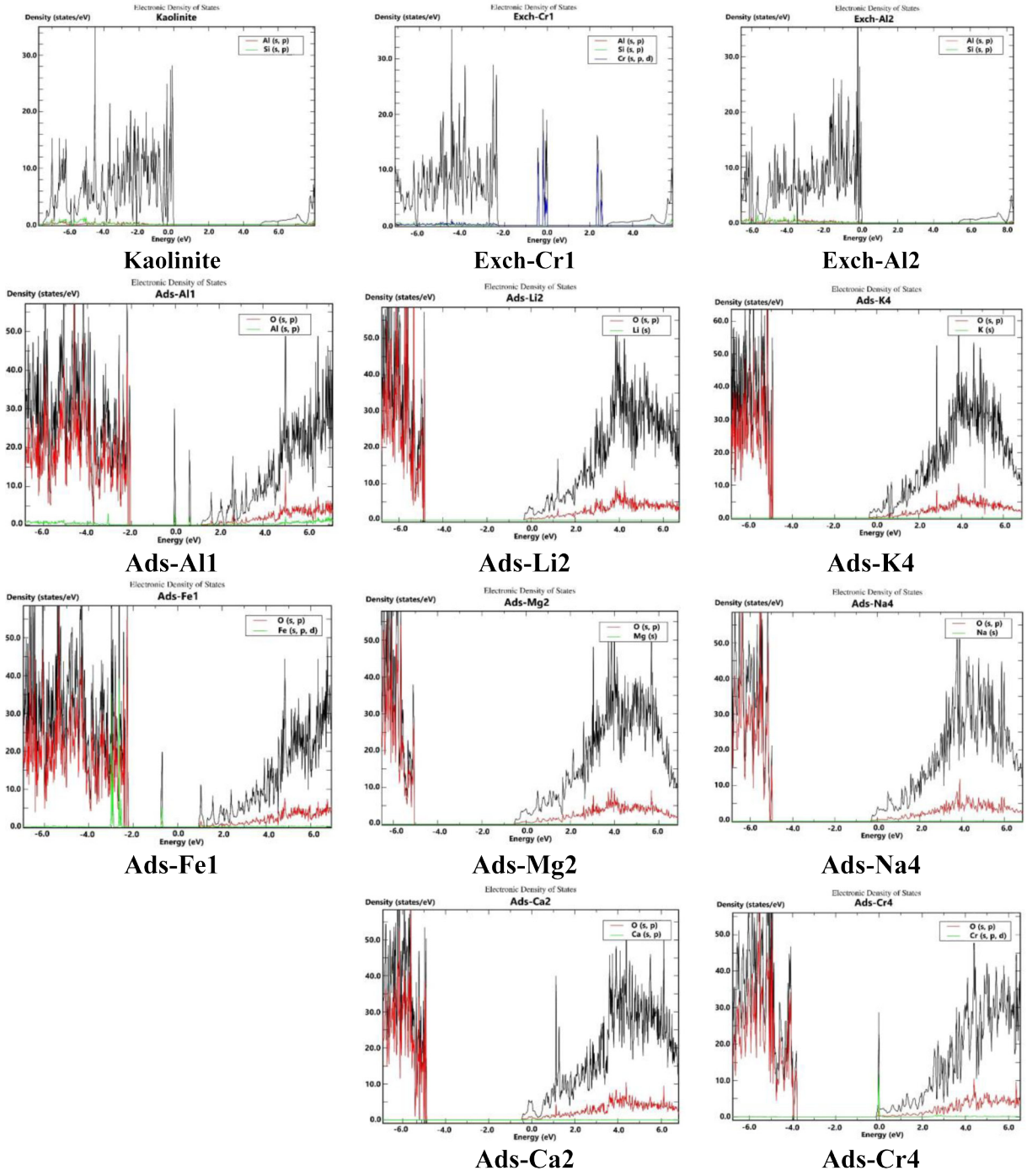

Figure 5. The pDOS of the most stable configurations for metal cations exchange and adsorption.

As shown in Figure 5, there are slight decreases in the density of states (DOS) in the valence band (VB) and conduction band (CB). These two shifts are approximate in most structures, so the gap energy (E_g) has little change compared to the initial kaolinite. Besides, in the exchange of Cr^{3+} at Al site (**Exch-Cr1**) and adsorption of Al^{3+}, Fe^{3+} on H-slab (**Ads-M1**), the hybridizations of the 3s, 3p (Al), 3d (Cr, Fe) orbitals and the 2s, 2p orbitals of O (in kaolinite) lead to form Al-O and Cr/Fe-O new bonds. It can be seen from new states as narrow lines between VB and CB. The band gaps of these structures are thus significantly reduced. Therefore, the Cr^{3+} exchange at the Al site and the Al^{3+}, Fe^{3+} adsorption at the H-slab would yield better light absorption and increase the photocatalytic activity of the materials compared to the original kaolinite.

4. CONCLUSIONS

Theoretical results indicate that the cation exchanges into the lattice structure of kaolinite are unfavorable and endothermic. The adsorption of metal cations on planes of kaolinite is preferred on both H-slab and O-slab in forming M-O bonds. The Li^+, Mg^{2+}, and Ca^{2+} cations are adsorbed alternately to the H-slab and O-slab, in which Li^+ and Mg^{2+} favorably insert into the lattice structure of kaolinite. The Na^+, K^+, and Cr^{3+} ions interact strongly with O sites on the O-slab at the octahedral cage. In addition, Al^{3+} and Fe^{3+} are located firmly at the tetrahedral cage on the H-slab. Adsorptions of metal cations on kaolinite are regarded as chemisorption and follow the sequence: $Li^+ > K^+ > Na^+ > Ca^{2+} > Al^{3+} > Fe^{3+} > Cr^{3+} > Mg^{2+}$. The formation of configurations yields the changes in VB and CB regions and band gap energy. Noticeably, the considerable differences in DOS and band gaps are found in structures of Cr^{3+} exchange and Al^{3+}, Fe^{3+} adsorption as compared to the remaining cations. Besides, the ELF analysis determines the formation of the M-O covalent bonds, which contribute mainly to the stability of configurations.

Acknowledgment

This research is conducted within the framework of science and technology projects at the institutional level of Quy Nhon University under the project code T2023.797.07.

REFERENCES

1. R. G. Harris, J. D. Wells, B. B. Johnson. Selective adsorption of dyes and other organic molecules to kaolinite and oxide surfaces, *Colloids and Surfaces A: Physicochemical and Engineering Aspects*, **2001**, *180*, 131-140.
2. J. Chen, F. F. Min, L. Liu, C. Liu, F. Lu. Experimental investigation and DFT calculation of different amine/ammonium salts adsorption on kaolinite, *Applied Surface Science*, **2017**, *419*, 241-251.
3. S. Zhang, J. J. Sheng, Z. Qiu. Water adsorption on kaolinite and illite after polyamine adsorption, *Journal of Petroleum Science and Engineering*, **2016**, *142*, 13-20.
4. E. R. Johnson, O. D. L. R. Alberto. Adsorption of organic molecules on kaolinite from the exchange-hole dipole moment dispersion model, *Journal of Chemical Theory and Computation*, **2012**, *8*, 5124-5131.
5. J. Lain, Y. Foucaud, A. B. Petriciolet, M. Badawi. Molecular picture of the adsorption of phenol, toluene, carbon dioxide and water on kaolinite basal surfaces, *Applied Surface Science*, **2022**, *585*, 152699.
6. L. Liu, F. Min, J. Chen, F. Lu, L. Shen. The adsorption of dodecylamine and oleic acid on kaolinite surfaces: insights from DFT calculation and experimental investigation, *Applied Surface Science*, **2019**, *470*, 27.
7. F. Fang, F. Min, L. Liu, J. Chen, B. Ren, C. Liu. Adsorption of $Al(OH)_n^{(3-n)+}$ (n = 2–4) on kaolinite (001) surfaces: a DFT study, *Applied Clay Science*, **2020**, *187*, 10545.
8. H. Wu, Y. Miao, Y. Li, H. Yan, J. Tan, S. Qiu, H. Wu, T. Qiu. Density functional theory study on the adsorption of $Fe(OH)_{2+}$ on kaolinite surface in water environment, *Processes*, **2023**, *11*, 38.

9. X. Wang, Y. Huang, Z. Pan, Y. Wang, C. Liu. Theoretical investigation of lead vapor adsorption on kaolinite surfaces with DFT calculations, *Journal of Hazardous Materials*, **2015**, *295*, 43-54.

10. D. J. Groenendijk. J. N. M. Wunnik. Surfactant adsorption and ion exchange on calcite surfaces, *Energy Fuels*, **2021**, *35*, 8763-8772.

11. A. F. A. Majid, R. Dewi, N. N. M. Shahri, E. W. E.S. Shahrin, E. Kusrini, N. Shamsuddin, J. W. Lim, S. Thongratkaew, K. Faungnawakij, A. Usman. Enhancing adsorption performance of alkali activated kaolinite in the removal of antibiotic rifampicin from aqueous solution, *Colloids and Surfaces A: Physicochemical and Engineering Aspects*, **2023**, *676*, 132209.

12. G. Chen, H. Zhao, X. Li, S. Xia. Theoretical insights into the adsorption mechanism of Cd(II) on the basal surfaces of kaolinite, *Journal of Hazardous Materials*, **2022**, *422*, 126795.

13. Z. Chen, Y. Zhao, D. Tong, S. Nie, Y. Wang, X. Nie, Z. Jia. A theoretical study of Cs(I) adsorption on kaolinite basal surfaces, *Chemical Physics*, **2022**, *553*, 111380.

14. J. Hafner. Ab-initio simulations of materials using VASP: density-functional theory and beyond, *Journal of Computational Chemistry*, **2008**, *29*(13), 2044-2078.

15. R. A. Young, A. W. Hewat. Verification of the triclinic crystal structure of kaolinite, *Clays and Clay Minerals*, **1988**, *36*(3), 225-232.

16. P. Perdew, K. Burke. Generalized gradient approximation made simple, *Physical Review Letters*, **1996**, *77*, 3865-3868.

17. C. E. White, J. L. Provis, T. Proffen, D. P. Riley, J. S. J. Deventer. Density functional modeling of the local structure of kaolinite subjected to thermal dehydroxylation, *Journal of Physical Chemistry A*, **2010**, *114*, 4988-4996.

18. M. C. He, J. Zhao, Z. J. Fang, P. Zhang. First-principles study of isomorphic ('dual-defect') substitution in kaolinite, *Clays and Clay Minerals*, **2011**, *59*(5), 501-506.

19. J. Luo, H. Yi, J. Wang, Z. Wang, B. Shen, J. Xu, L. Liu, Q. Shi, C. Huang. Effect of alkaline metals (Na, Ca) on heavy metals adsorption by kaolinite during coal combustion: experimental and DFT studies, *Fuel*, **2023**, *348*, 128503.

20. G. Chen, X. Li, H. Zhao, M. Qiu, S. Xia, L. Yu. Revealing the mechanisms of mercury adsorption on metal-doped kaolinite (001) surfaces by first principles, *Journal of Hazardous Materials*, **2022**, *431*, 128586.

21. K. Koumpouras, J. A. Larsson. Distinguishing between chemical bonding and physical binding using electron localization function (ELF), *Journal of Physics: Condensed Matter*, **2020**, *32*, 315502.

TẠP CHÍ KHOA HỌC
TRƯỜNG ĐẠI HỌC QUY NHƠN

Tính chất Forelli mạnh của các không gian Fréchet và định lí Alexander đối với các chuỗi lũy thừa hình thức giá trị Fréchet

Nguyễn Văn Đại*

Khoa Sư phạm, Trường Đại học Quy Nhơn, Việt Nam

Ngày nhận bài: 18/10/2023; Ngày sửa bài: 03/01/2024
Ngày nhận đăng: 19/01/2024; Ngày xuất bản: 28/06/2024

TÓM TẮT

Chúng tôi đưa ra các điều kiện đủ để một chuỗi luỹ thừa hình thức (tương ứng, một dãy của chuỗi luỹ thừa hình thức) của các đa thức thuần nhất, liên tục, giá trị Fréchet hội tụ trong lân cận của 0 trên không gian Fréchet E (tương ứng, $E = \mathbb{C}^N$) là hội tụ trong lân cận của 0 trên mỗi đường thẳng phức $\ell_a := \mathbb{C}a$ với mỗi $a \in A$ (A là tập không đa cực xạ ảnh trong $\mathbb{C}^N$). Kết quả trong trường hợp $E = \mathbb{C}^N$ là một "phiên bản giá trị Fréchet" của định lý Alexander cổ điển nhưng với các giả thiết yếu hơn. Chúng tôi cũng chứng minh rằng mọi không gian Fréchet F có tính chất Forelli mạnh, nghĩa là nếu mọi hàm $f : \Delta_N \to F$ sao cho $f \in C^\infty(0)$ và $f|_{l_a \cap \Delta_N}$ là chỉnh hình với mọi đường thẳng phức $l_a, a \in A$, thì f chỉnh hình trên Δ_N.

Từ khóa: *Hàm đa điều hoà dưới, hàm chỉnh hình, tập đa cực xạ ảnh, chuỗi luỹ thừa hình thức.*

**Tác giả liên hệ chính.*
Email: nguyenvandai@qnu.edu.vn

QUY NHON UNIVERSITY
JOURNAL OF SCIENCE

Strong Forelli property of Fréchet spaces and Alexander's theorem for Fréchet-valued formal power series

Nguyen Van Dai*

Faculty of Education, Quy Nhon University, Vietnam

Received: 18/10/2023; Revised: 03/01/2024
Accepted: 19/01/2024; Published: 28/06/2024

ABSTRACT

We give sufficient conditions to ensure the convergence on some zero-neighbourhood in a Fréchet space E (resp. $E = \mathbb{C}^N$) of a formal power series (resp. a sequence of formal power series) of Fréchet-valued continuous homogeneous polynomials provided that the convergence holds at a zero-neighbourhood of each complex line $\ell_a := \mathbb{C}a$ for every $a \in A$, a non-projectively-pluripolar set in E. The result in the case $E = \mathbb{C}^N$ is a Fréchet-valued analog of classical Alexander's theorem but under weaker assumptions. It is also shown that every Fréchet space has the strong Forelli property, i.e, for a non-projectively-pluripolar set $A \subset \mathbb{C}^N$, every Fréchet-valued function f on the open unit ball $\Delta_N \subset \mathbb{C}^N$, $f \in C^\infty(0)$, such that its restriction on each complex line ℓ_a, $a \in A$, is holomorphic admits an extension to an entire function.

Keywords: *Plurisubharmonic functions, holomorphic functions, projectively pluripolar sets, formal power series.*

1. INTRODUCTION AND PRELIMINARIES

The focus of this paper is to study the Fréchet-valued analogs and the generalizations of the following two classical theorems.

Forelli's Theorem. [1] *If f is a function defined in the unit ball $\Delta_N \subset \mathbb{C}^N$, holomorphic on the intersection of Δ_N with every complex line ℓ passing through the origin and if f is of class C^∞ in a neighborhood of this point, then it is holomorphic in Δ_N.*

Alexander's Theorem. [2] *Let $\mathscr{F}$ be a family of analytic functions on $\Delta_N \subset \mathbb{C}^N$. If the restriction of $\mathscr{F}$ to each complex line through the origin is normal (resp. at the origin), then $\mathscr{F}$ is normal (resp. at the origin).*

Recall that a family $\mathscr{F}$ of analytic functions on a complex manifold Ω is *normal* if every sequence in $\mathscr{F}$ has a subsequence which converges uniformly on compact subsets of Ω either to an analytic function or to ∞, and that $\mathscr{F}$ is normal at a point $x \in \Omega$ if there exists a neighborhood W of x such that the restriction of $\mathscr{F}$ to W is normal.

Forelli's theorem is a radial analogue of the fundamental theorem of Hartogs. Alexander's theorem allows us to obtain the Hartogs theorem on the convergence of formal power series in several complex variables.

*Corresponding author.
Email: nguyenvandai@qnu.edu.vn

https://doi.org/10.52111/qnjs.2024.18302

The problems of extensions and generalizations of the above classical theorems for holomorphic maps and vector-valued holomorphic functions have drawn attention of mathematicians.

In this note, we will investigate these results for the Fréchet-valued case in the "strong" sense in which the functions are only required that their restrictions on $\ell \cap \Delta_N$ are holomorphic for every $\ell \in \mathscr{L}$, *a family of sufficiently many complex lines* passing through the origin.

Families of "sufficiently many" complex lines in the paper concern the notions of pluripolar sets and projectively pluripolar sets. These notions require some extra background material for their definition.

Let D be a domain in a locally convex space E. An upper-semicontinuous function $\varphi : D \to [-\infty, +\infty)$ is said to be *plurisubharmonic*, and write $\varphi \in PSH(D)$, if φ is subharmonic on every one dimensional section of D.

A subset $B \subset D$ is said to be *pluripolar* in D if there exists $\varphi \in PSH(D)$ such that $\varphi \not\equiv -\infty$ and $\varphi\big|_B = -\infty$.

A function $\varphi \in PSH(E)$ is called *homogeneous plurisubharmonic* if

$$\varphi(\lambda z) = \log|\lambda| + \varphi(z) \quad \forall \lambda \in \mathbb{C},\ \forall z \in E.$$

We denote by $HPSH(E)$ the set of homogeneous plurisubharmonic functions on E. We say that a subset $A \subset E$ is *projectively pluripolar* if A is contained in the $-\infty$ locus of some element in $HPSH(E)$ which is not identically $-\infty$. It is clear that projective pluripolarity implies pluripolarity. The converse is not true (see [3] [Proposition 3.2 b]).

Some properties, examples and counterexamples of projectively pluripolar sets may be found in the article. [3] We introduce below a few examples in locally convex spaces.

Example 1.1. Let E be a metrizable locally convex space. Fix $a \in E$. Then, the complex line $\ell_a := \mathbb{C}a = \{\lambda a : \lambda \in \mathbb{C}\}$, hence, every $A \subset \ell_a$, is projectively pluripolar in E.

Indeed, let d be the metric defining the topology on E. Consider the function

$$\varphi(z) = -\log d(z, \ell_a) := -\log \inf_{w \in \ell_a} d(z, w).$$

It is easy to check that $\varphi \in HPSH(E)$, $\varphi \not\equiv -\infty$ and $\ell_a \subset \varphi^{-1}(-\infty)$.

Example 1.2. Let E be a Fréchet space which contains a non-pluripolar compact balanced convex subset B. By the same proof as in Example 1.1, the set ∂B is pluripolar. However, ∂B is not projectively pluripolar in E.

Otherwise, we can find a function $\varphi \in HPSH(E)$, $\varphi \not\equiv -\infty$ and $\partial B \subset \varphi^{-1}(-\infty)$. For every $z \in B$ we can write $z = \lambda y$ for some $y \in \partial B$ and $|\lambda| < 1$. Then

$$\varphi(z) = \varphi(\lambda y) = \log|\lambda| + \varphi(y) = -\infty,\ \forall z \in B.$$

It is impossibe because B is non-pluripolar.

Example 1.3. By Theorem 9 of the research [4] and Example 1.2, a nuclear Fréchet space having the linear topological invariant $(\widetilde{\Omega})$ which is introduced by Vogt (see [5]) contains a non-projectively-pluripolar set.

We recall that a complex space or a locally convex space X is said to have *Forelli Property* if every map $f : \Delta_N \to X$ such that f is of C^∞- class in a neighborhood of $0 \in \Delta_N$ and $f\big|_{\ell \cap \Delta_N}$ is holomorphic for *all* complex lines ℓ through $0 \in \Delta_N$ then f is holomorphic on Δ_N. In 2005 L. M. Hai and N. V. Khue [6] studied the Forelli property for complex spaces. They also investigated the relation between these spaces with Hartogs spaces and Hartogs holomorphic extension spaces for holomorphically convex Kähler complex spaces.

Definition 1.1. A locally convex space F is said to have the *strong Forelli property* if every function $f : \Delta_N \to F$ satisfying that:

(i) f belongs to C^k-class at $0 \in \mathbb{C}^N$ for $k \geq 0$,

(ii) for some non-projectively-pluripolar subset $A \subset \mathbb{C}^N$, the restriction of f on each complex line ℓ_a, $a \in A$, is holomorphic,

then there exists an entire function $\widehat{f}$ on $\mathbb{C}^N$ such that $\widehat{f} = f$ on ℓ_a for all $a \in A$.

Note that, from Proposition 3.1 in the research, [3] in $\mathbb{C}^N$, the following are equivalent:

a) A is projectively pluripolar;

b) $A^\lambda := \{tz : \ t \in \mathbb{C}, |t| < \lambda, z \in A\}$ is pluripolar for each $\lambda > 0$;

c) $\mu(A^\lambda) = 0$ where μ is the Lebesgue measure;

d) $\nu(\varrho(A^\lambda)) = 0$ where ν is the invariant measure on the projective space $\mathbb{CP}^{N-1}$ and $\varrho : \mathbb{C}^N \setminus \{0\} \to \mathbb{CP}^{N-1}$ is the natural projection.

It follows that the condition (ii) in Definition 1.1 can be replaced by the following condition:

(ii') for some family $\mathscr{L}$ of complex lines through $0 \in \mathbb{C}^N$ such that $\mu\big(\Delta_N \cap \bigcup_{\ell \in \mathscr{L}} \ell\big) > 0$, the restriction of f on each $\ell \in \mathscr{L}$ is holomorphic.

The main theorems of our note are the following.

Theorem 1.1. *Every Fréchet space has the strong Forelli property.*

Theorem 1.2. *Let $A \subset \mathbb{C}^N$ be a non-projectively-pluripolar set and $(f_n)_{n\geq 1}$ be a sequence of formal power series of continuous homogeneous polynomials on $\mathbb{C}^N$ with values in a Fréchet space. Assume that there exists $r_0 \in (0,1)$ such that, for each $a \in A$, the restriction of $(f_n)_{n\geq 1}$ on ℓ_a is a sequence of holomorphic functions which is convergent on the disk $\Delta(r_0)$. Then there exists $r > 0$ such that $(f_n)_{n\geq 1}$ is a sequence of holomorphic functions that converges on $\Delta_N(r)$.*

By the equivalence of a) and d) mentioned above, the hypotheses of Theorem 1.2 may be stated under an alternative form as follows: *Let B be a subset of Δ_N such that $\nu(\varrho(B)) = 0$ where ν is the invariant measure on the projective space $\mathbb{CP}^{N-1}$ and $\varrho : \mathbb{C}^N \setminus \{0\} \to \mathbb{CP}^{N-1}$ is the natural projection. Assume that for some $r_0 \in (0,1)$, the restriction of the sequence $(f_n)_{n\geq 1}$ on each complex line ℓ through $0 \in \Delta_N$ with $\ell \cap B = \{0\}$ is convergent in $\Delta(r_0)$.*

Actually, Theorem 1.2 is not a generalization of Alexander's theorem because our result only refers to uniform convergence, not to the normality of the sequence of formal power series. Therefore, it is still an *open question* that whenever we obtain a truly generalization of Alexander's theorem. In other words, "*Whether or not a version of Theorem 1.2 where the uniform convergence of the sequence $(f_n|_{\ell_a})_{n\geq 1}$ on compact sets of $\Delta(r_0)$ is replaced by* normality *of this sequence on $\Delta(r_0)$ i.e., we allow convergence to ∞ uniformly on compact sets?*"

The proof of the first main theorem will be presented in Section 2. To prepare for the proof, with the help of techniques of pluripotential theory and functional analysis, we investigate the Hartogs Lemma for sequence of plurisubharmonic functions for the infinite dimensional case (Theorem 2.2). This result is also essential to the Section 3 in which we discus a problem closely related to the two classical theorems mentioned above. The main goal of this section (Theorem 3.1) is to study the convergence set of a formal power series of continuous homogeneous polynomials between Fréchet spaces under the hypothesis that it is convergent along a pencil of complex lines through the origin.

Finally, the last section presents the proof of the second main theorem of the paper. Some results concerning to Vitali's theorem for a sequence of Fréchet-valued holomorphic

https://doi.org/10.52111/qnjs.2024.18302

functions (Proposition 4.3) will be shown to help for our proof.

The standard notation of the theory of locally convex spaces used in this note is presented as in the book of Jarchow. [7] A locally convex space is always a complex vector space with a locally convex Hausdorff topology. For a locally convex space E we use E'_{bor} to denote E' equipped with the bornological topology associated with the strong topology β.

The locally convex structure of a Fréchet space is always assumed to be generated by an increasing system $(\|\cdot\|_k)_{k\geq 1}$ of seminorms. For an absolutely convex subset B of E, by E_B we denote the linear hull of B which becomes a normed space in a canonical way if B is bounded (with the norm $\|\cdot\|_B$ is the gauge functional of B).

We say that a Fréchet space E has the property (LB_∞), and write $E \in (LB_\infty)$ for short, if $\forall \varrho_N \uparrow \infty, \exists p\, \forall q\, \exists k(q) \geq q$, $C(q) > 0, \forall x \in E, \exists m$ with $q \leq m \leq k(q)$:

$$\|x\|_q^{1+\varrho_m} \leq C(q)\|x\|_m \|x\|_p^{\varrho_m}.$$

This property is a linear toplogical invariant which plays a very important role in modern theory of Fréchet spaces. Khue, Hai, Hoan [8] [Theorem 4.1] proved that if $E \in (LB_\infty)$ then $(E'_{\text{bor}})'_\beta \in (LB_\infty)$.

For further terminology from complex analysis we refer to the research. [9]

We use throughout this paper the following notations: $\Delta_N(r) = \{z \in \mathbb{C}^N : \|z\| < r\}$; $\Delta_N := \Delta_N(1); \Delta(r) = \Delta_1(r)$; $\Delta := \Delta_1$; and ℓ_a is the complex line $\mathbb{C}a$.

2. THE STRONG FORELLI PROPERTY OF FRÉCHET SPACES

This section is devoted to the proof of Theorem 1.1. First we investigate the Hartogs Lemma for a sequence of plurisubharmonic functions in the infinite dimensional case. This is essential to our proofs.

Lemma 2.1. *Let $(P_n)_{n\geq 1}$ be a sequence of continuous homogeneous polynomials on a Baire locally convex space E of degree $\leq n$. Assume that*

$$\limsup_{n\to\infty} \frac{1}{n} \log |P_n(z)| \leq 0$$

for each $z \in E$. Then for every $\varepsilon > 0$ and every compact set K in E there exists n_0 such that

$$\frac{1}{n} \log |P_n(z)| < \varepsilon \quad \forall n > n_0,\ \forall z \in K.$$

Proof. Since

$$\limsup_{n\to\infty} |P_n(z)|^{\frac{1}{n}} \leq 1 \quad \forall z \in E$$

the formula

$$f(z)(\lambda) = \sum_{n\geq 1} P_n(z)\lambda^n$$

defines a function $f : E \to H(\Delta)$, the Fréchet space of holomorphic functions on the open unit disc $\Delta \subset \mathbb{C}$.

Let us check f is holomorphic on E. Given $z \in E \setminus \{0\}$ and consider $f(\cdot\, z) : \mathbb{C} \to H(\Delta)$ with

$$f(\xi z)(\lambda) = \sum_{n\geq 1} P_n(z)\lambda^n \xi^{k_n}$$

where $k_n = \deg P_n \leq n$. Then $f(\cdot\, z)$ is holomorphic because for $0 < r < 1$ we have

$$\begin{aligned}
&\lim_{n\to\infty} \sup_{|\lambda|\leq r} (|P_n(z)||\lambda|^n)^{\frac{1}{k_n}} \\
&= \limsup_{n\to 0} (|P_n(z)|^{\frac{1}{n}} r)^{\frac{n}{k_n}} \\
&\leq \limsup_{n\to 0} |P_n(z)|^{\frac{1}{n}} r \leq r < 1.
\end{aligned}$$

This means that f is Gâteaux holomorphic on E.

Now for each $k \geq 1$ we put

$$A_k := \{z \in E :\ |P_n(z)| \leq k^{k_n} \quad \forall n \geq 1\}.$$

By the continuity of P_n, the sets A_k are closed in E. Moreover, $E = \bigcup_{k\geq 1} A_k$. Since E is a Baire space, there exists $k_0 \geq 1$ such that $\text{Int}A_{k_0} \neq \varnothing$. Then f is holomorphic on $\frac{1}{k_0}\text{Int}A_{k_0}$ because

$$\sum_{n\geq 1} |P_n(z)||\lambda|^n \leq \sum_{n\geq 1} \frac{k_0^{k_n}}{k_0^{k_n}} r^n = \sum_{n\geq 1} r^n < \infty$$

https://doi.org/10.52111/qnjs.2024.18302

for $0 < r < 1$. Hence, by Zorn's theorem [10] [Theorem 1.3.1], f is holomorphic on E.

Now given $K \subset E$ a compact set and $\varepsilon > 0$. Take $0 < r < 1$ and denote

$$C := \sup\{|f(z)(\lambda)| : \ z \in K, |\lambda| \le r\} < \infty.$$

Then we have

$$|P_n(z)| = \left| \frac{1}{2\pi i} \int_{|\xi|=r} \frac{f(z)(\xi) d\xi}{\xi^{n+1}} \right| \le \frac{C}{r^n} \ \forall z \in K,$$

i.e,

$$|P_n(z)|^{\frac{1}{n}} \le \frac{C^{\frac{1}{n}}}{r}.$$

Choose n_0 sufficiently large we obtain

$$|P_n(z)|^{\frac{1}{n}} \le \frac{C^{\frac{1}{n}}}{r} < e^{\varepsilon} \quad \forall n > n_0.$$

The lemma is proved. □

The Proposition 5.2.1 in the research [11] says that a non-empty family $(u_\alpha)_{\alpha \in I}$ of plurisubharmonic functions from the Lelong class such that the set $\{z \in \mathbb{C}^N : \sup_{\alpha \in I} u_\alpha(z) < \infty\}$ is not $\mathcal{L}$-polar is locally uniformly bounded from above.

The next is similar to the above result in the infinite dimensional case.

Theorem 2.2. *Let B be a balanced convex compact subset of a Fréchet space E and $(P_n)_{n \ge 1}$ be a sequence of continuous homogeneous polynomials on E of degree $\le n$. Assume that the set*

$$\left\{ z \in E_B : \sup_{n \ge 1} \frac{1}{n} \log |P_n(z)| < \infty \right\}$$

is not projectively pluripolar in E_B. Then the family $(\frac{1}{n} \log |P_n|)_{n \ge 1}$ is locally uniformly bounded from above on E_B.

Proof. Suppose that the family $(\frac{1}{n} \log |P_n|)_{n \ge 1}$ is not locally uniformly bounded from above on B. Then there exists a sequence $(u_j)_{j \ge 1} = (\frac{1}{n_j} \log |P_{n_j}|)_{j \ge 1}$ such that

$$M_j := \sup_{z \in B} u_j(z) \ge j \quad \forall j \ge 1.$$

Take $w \in E_B \setminus B$ and for each $j \ge 1$ consider the function

$$v_j(\zeta) := u_j(\zeta^{-1} w) - M_j - \log^+(|\zeta|^{-1} \|w\|_B),$$

for $\zeta \in \Delta(\|w\|_B) \setminus \{0\}$. Obviously, v_j is subharmonic and, it is easy to see that $v_j(\zeta) \le O(1)$ as $\zeta \to 0$. Hence, in view of Theorem 2.7.1 in [11], v_j extends to a subharmonic function, say $\widetilde{v}_j$, on $\Delta(\|w\|_B)$. Now, by the maximum principle, $\widetilde{v}_j \le 0$ on $\Delta(\|w\|_B)$. In particular,

$$v_j(1) = \widetilde{v}_j(1) = u_j(w) - M_j - \log^+ \|w\|_B \le 0.$$

Hence

$$u_j(z) - M_j \le \log^+ \|z\|_B \quad \text{for } z \in E_B, \forall j \ge 1. \tag{2.1}$$

Then there exists $z_0 \in E_B$ such that

$$\limsup_{j \to \infty} \exp\left(u_j(z_0) - M_j\right) =: \delta > 0. \tag{2.2}$$

For otherwise we would have

$$\limsup_{j \to \infty} \exp(u_j(z) - M_j) \le 0$$

at each point $z \in E_B$. By Lemma 2.1, the sequence $(\exp(u_j(z) - M_j))_{j \ge 1}$ is bounded from above on any compact set in E_B. This would imply from the research [10][Lemma 1.1.12] that $\exp\left(u_j(z) - M_j\right) < \frac{1}{2}$ for all $z \in B$ and all sufficiently large j. But then the last estimate would contradict the definition of the constants M_j.

Now we choose a subsequence $(u_{j_k})_{k \ge 1} \subset (u_j)_{j \ge 1}$ such that

$$\lim_{k \to \infty} \exp(u_{j_k}(z_0) - M_{j_k}) = \delta \quad \text{and} \quad M_{j_k} \ge 2^k$$

for all $k \ge 1$. Consider the function

$$w(z) := \sum_{k \ge 1} 2^{-k} (u_{j_k} - M_{j_k}), \quad z \in E_B.$$

In view of (2.1) we have the extimate

$$w_k(z) := 2^{-k}(u_{j_k} - M_{j_k}) - 2^{-k} \log R \le 0$$

for $z \in E_B$, $\|z\|_B \le R$ and $R \ge 1$. Thus w_k is plurisubharmonic on $\{z \in E_B : \ \|z\|_B < R\}$ and $w_k \le 0$. Hence, the function $\sum_{k \ge 1} w_k =$

https://doi.org/10.52111/qnjs.2024.18302

$w - \log R$, $R > 1$, is either plurisubharmonic on $\{z \in E_B : \|z\|_B < R\}$ or identically $-\infty$. Consequently, as R can be chosen arbitrarily large, w is either plurisubharmonic or identically $-\infty$. Therefore, since $w(z_0) > -\infty$, $w \in PSH(E_B)$. It is easy to see that $w \in HPSH(E_B)$.

If $z \in E_B$, $\sup_{n\geq 1} \frac{1}{n}\log|P_n(z)| < \infty$ then $\sum_{k\geq 1} 2^{-k}u_{j_k}(z) < \infty$ and, hence

$$w(z) \leq \sum_{k\geq 1} 2^{-k}u_{j_k}(z) - \sum_{k\geq 1} 1 = -\infty$$

which proves that the set

$$\left\{z \in E_B : \sup_{n\geq 1} \frac{1}{n}\log|P_n(z)| < \infty\right\}$$

is projectively pluripolar in E_B. This contradics the hypothesis. □

Corollary 2.3. *Let B, E and $(P_n)_{n\geq 1}$ be as in Theorem 2.2; in addition assume that B contains a non-projectively-pluripolar subset. Then the family $(\frac{1}{n}\log|P_n|)_{n\geq 1}$ is locally uniformly bounded from above on E.*

Proof. It suffices to prove that E_B is dense in E. Indeed, if the closure of the subspace E_B is not equal to E then, by the Hahn-Banach theorem, there exists $\varphi \in E'$, $\varphi \neq 0$, such that $\varphi(E_B) = 0$. Then it is easy to see that $v := \log|\varphi| \in HPSH(E)$, $v \not\equiv 0$, $B \subset E_B \subset \{z : v(z) = -\infty\}$. This contradicts the fact that B contains a non-projectively-pluripolar subset. □

It is known that a subset with non-empty interior in a Fréchet space is not pluripolar, hence it is not projectively pluripolar. Then by Corollary 2.3 we have the following.

Corollary 2.4. *Let B be a balanced convex compact subset of a Fréchet space E which contains a non-projectively-pluripolar subset and $(P_n)_{n\geq 1}$ be a sequence of continuous homogeneous polynomials on E of degree $\leq n$. If the set*

$$\left\{z \in E_B : \sup_{n\geq 1} \frac{1}{n}\log|P_n(z)| < \infty\right\}$$

has the non-empty interior in E then the family $(\frac{1}{n}\log|P_n|)_{n\geq 1}$ is locally uniformly bounded from above on E.

We are now in a position to prove the first main theorem.

Proof of Theorem 1.1. Let F be a Fréchet space, $f : \Delta_n \to F$ be a function which belongs to C^k-class at $0 \in \mathbb{C}^n$ for $k \geq 0$ and $A \subset \mathbb{C}^n$ be a non-projectively-pluripolar set. If the restriction of f on each complex line ℓ_a, $a \in A$, is holomorphic. By the hypothesis, for each $k \geq 0$ there exists $r_k \in (0, 1)$ such that f is a C^k-function on $\Delta_N(r_k)$. We may assume that $r_k \searrow 0$. Put

$$P_k(z) = \frac{1}{2\pi i}\int_{|\lambda|=1} \frac{f(\lambda z)d\lambda}{\lambda^{k+1}}, \quad z \in \Delta_N(r_k).$$

Then, for each $k \geq 0$ and $p \geq k$, P_m is a bounded C^p-function on $\Delta_N(r_p)$. Since $\lambda \mapsto f(\lambda a)$ is holomorphic for all $a \in A$ we deduce that

$$P_k(\lambda a) = \lambda^k P_k(a) \quad \text{for } a \in A, \lambda \in \mathbb{C}. \quad (2.3)$$

By the boundedness of P_k on $\Delta_N(r_k)$ we have

$$P_k(w) = O(|w|^k) \quad \text{as } w \to 0.$$

On the other hand, since $P_k \in C^{k+1}(\Delta_N(r_{k+1}))$, the Taylor expansion of P_k at $0 \in \Delta_N(r_{k+1})$ has the form

$$P_k(z) = \sum_{\alpha+\beta=k} P_{k,\alpha,\beta}(z) + |z|^k\varrho(z) \quad (2.4)$$

where $P_{k,\alpha,\beta}$ is a polynomial of degree α in z and degree β in $\overline{z}$ and $\varrho(z) \to 0$ as $z \to 0$.

In (2.4), replacing z by λz, $|\lambda| < 1$, from (2.3) we obtain

$$\sum_{\alpha+\beta=k} P_{k,\alpha,\beta}(z)\lambda^\alpha\overline{\lambda}^\beta + |\lambda|^k|z|^k\varrho(\lambda z)$$

$$= \sum_{\alpha+\beta=k} P_{k,\alpha,\beta}(z)\lambda^k + \lambda^k|z|^k\varrho(z) \quad (2.5)$$

for $z \in r_{k+1}A$.

This yields that $\varrho(\lambda z) = \varrho(z)$ for $\lambda \in [0,1)$, and hence, $\varrho(z) = \varrho(0) = 0$ for $z \in r_{k+1}A$. Thus

$$P_{k,\alpha,\beta}(z) = 0 \quad \text{for } \beta > 0 \text{ and } z \in r_{k+1}A.$$

Note that $r_{k+1}A$ is also not projectively pluripolar. It is easy to check that

$$P_{k,\alpha,\beta} = 0 \quad \text{for } \beta > 0.$$

Indeed, for every $\varphi \in F'$, the function

$$u(w) = \frac{1}{\deg P_{k,\alpha,\beta}} \log |(\varphi \circ P_{k,\alpha,\beta})(w)|$$

is homogeneous plurisubharmonic on $\mathbb{C}^N$, $u \equiv -\infty$ on $r_{k+1}A$. Since $r_{k+1}A$ is not projectively pluripolar, it implies that $u \equiv -\infty$ and hence $\varphi \circ P_{k,\alpha,\beta} \equiv 0$ on $\mathbb{C}^N$ for every $\varphi \in F'$. It implies that $P_{k,\alpha,\beta} \equiv 0$ on $\mathbb{C}^N$ for $\beta > 0$.

Thus, from (2.4) we have

$$P_k(z) = P_{k,k,0}(z) = \sum_{|\alpha|=k} c_\alpha z^\alpha$$

for $z \in \Delta_N(r_{k+1})$ and P_k is a homogeneous holomorphic polynomial of degree k.

Now, let $(\|\cdot\|_m)_{m\geq 1}$ be an increasing fundamental system of continuous semi-norms defining the topology of F. By the hypothesis, for every $m \geq 1$

$$\limsup_{k\to\infty} \frac{1}{k} \log \|P_k(z)\|_m = -\infty \quad \text{for } z \in A.$$

Then, by Corollary 2.3, the sequence $(\frac{1}{k} \log \|P_k(z)\|_m)_{k\geq 1}$ is locally uniformly bounded from above on $\mathbb{C}^n$ for all $m \geq 1$. Thus we can define

$$u_m(z) = \limsup_{k\to\infty} \frac{1}{k} \log \|P_k(z)\|_m, \quad z \in \mathbb{C}^N.$$

By the research, [12] the upper semicontinuous regularization u_m^* of u_m belongs to the Lelong class $\mathcal{L}(\mathbb{C}^N)$ of plurisubharmonic functions with logarithmic growth on $\mathbb{C}^N$. Moreover, by Bedford-Taylor's theorem [13]

$$S_m := \{z \in \mathbb{C}^N : \ u_m^*(z) \neq u_m(z)\}$$

is pluripolar for all $m \geq 1$.

On the other hand, by [3], $A^* := \{ta : \ t \in \mathbb{C}, a \in A\}$ is not pluripolar. This yields that $u_m^* \equiv -\infty$ for all $m \geq 1$ because $u_m^* = u_m = -\infty$ on $A^* \setminus S_m$ and $A^* \setminus S_m$ is non-pluripolar. Since $u_m^* \geq u_m$ we have $u_m \equiv -\infty$ for $m \geq 1$. Hence the series $\sum_{k\geq 0} P_k(z)$ is convergent for $z \in \mathbb{C}^N$ and it defines a holomorphic extension $\widehat{f}$ of $f\big|_{\ell_a}$ for every $a \in A$. □

3. THE CONVERGENCE OF A FORMAL POWER SERIES BETWEEN FRÉCHET SPACES

In mathematics, a formal power series is a generalization of polynomials as a formal object, where the number of terms is allowed to be infinite.

The theory of formal power series has drawn attention of mathematicians working in different branches because of their various applications. One can find applications of formal power series in classical mathematical analysis and in the theory of Riordan algebras. Specially, this theory lays the foundation for substantial parts of combinatorics and real and complex analysis.

A formal power series $f(z_1, \ldots, z_N) = \sum c_{\alpha_1,\ldots,\alpha_N} z_1^{\alpha_1} \ldots z_N^{\alpha_N}$ in $\mathbb{C}^N$, $N \geq 2$, with coefficients in $\mathbb{C}$ is said to be convergent if it converges absolutely in a zero-neighborhood in $\mathbb{C}^N$. A classical result of Hartogs [14] states that a series f converges if and only if $f_z(t) = f(tz_1, \ldots, tz_N)$ converges, as a series in t, for all $z = (z_1, \ldots, z_N) \in \mathbb{C}^N$. In other words, a formal power series in several complex variables is convergent if it converges on *all* lines through the origin. This can be interpreted as a formal analog of Hartogs' theorem on separate analyticity. Because a divergent power series still may converge in certain directions, it is natural and desirable to consider the set of all $z \in \mathbb{C}^N$ for which f_z converges. Since $f_z(t)$ converges if and only if $f_w(t)$ converges for all $w \in \mathbb{C}^N$ on the affine line through z,

https://doi.org/10.52111/qnjs.2024.18302

ignoring the trivial case $z = 0$, the set of directions along which f converges can be identified with a subset of the projective space $\mathbb{CP}^{N-1}$. The convergence set $\mathrm{Conv}(f)$ of a divergent power series f is defined to be the set of all directions $\xi \in \mathbb{CP}^{N-1}$ such that $f_z(t)$ is convergent for some $z \in \varrho^{-1}(\xi)$ where $\varrho : \mathbb{C}^N \setminus \{0\} \to \mathbb{CP}^{N-1}$ is the natural projection. In the two-variables case, Lelong [15] proved that $\mathrm{Conv}(f)$ is an F_σ-polar set (i.e. a countable union of closed sets of vanishing logarithmic capacity) in $\mathbb{CP}^1$, and moreover, every F_σ-polar subset of $\mathbb{CP}^1$ is contained in the $\mathrm{Conv}(g)$ of some formal power series g. The optimal result was later obtained by Sathaye [16] who showed that the class of convergence sets of divergent power series in two-variables is precisely the class of F_σ-polar sets in $\mathbb{CP}^1$. Levenberg and Molzon, in [17], showed that if the restriction of f on sufficiently many (non-pluripolar) sets of complex line passing through the origin is convergent on small neighborhood of $0 \in \mathbb{C}$ then f is actually represent a holomorphic function near $0 \in \mathbb{C}^N$. By using delicate estimates on volume of complex varieties in projective spaces, Alexander's theorem mentioned above was proved. This follows readily that if the restriction of a formal power series f on every complex line passing through the origin in $\mathbb{C}^N$ is convergent then f is convergent [2] [Theorem 6.3].

The main result of this section is following.

Theorem 3.1. *Let A be a non-projectively-pluripolar set which is contained in a balanced convex compact subset of a Fréchet space E and $f = \sum_{n\geq 1} P_n$ be a formal power series where P_n are continuous homogeneous polynomials of degree n on E with values in a Fréchet space F. Assume that for each $a \in A$, the restriction of f on the complex line ℓ_a is convergent. Then f is convergent in a neighbourhood of $0 \in E$ if one of the following holds:*

(a) E is Schwartz.

(b) $F \in (LB_\infty)$.

Proof. We divide the proof into three steps:

(i) *Step 1: We consider the case where $F = \mathbb{C}$.* It follows from the hypothesis that

$$\limsup_{n\to\infty} |P_n(z)|^{\frac{1}{n}} < \infty \quad \forall z \in A.$$

Then, by Corollary 2.3 there exists a zero-neighbourhood U in E such that

$$\sup\{|P_n(z)|^{\frac{1}{n}} : \ z \in U, n \geq 1\} =: M < \infty.$$

This implies that f is uniformly convergent on $(2M)^{-1}U$.

(ii) *Step 2: We consider the case where F is Fréchet.* By the step 1 we can define the linear map

$$T : F'_{\mathrm{bor}} \to H(0_E)$$

by letting

$$T(u) = \sum_{n\geq 1} u(P_n)$$

where $H(0_E)$ denotes the space of germs of scalar holomorphic functions at $0 \in E$. Suppose that $u_\alpha \to u$ in F'_{bor} and $T(u_\alpha) \to v$ in $H(0_E)$ as $\alpha \to \infty$. This implies, in particular, that $[T(u_\alpha)](z) \to v(z)$ for all z in some zero-neighbourhood U in E. However, for $z \in U$ we have

$$\begin{aligned}
[T(u_\alpha - u)](z) &= \sum_{n\geq 1} (u_\alpha - u)(P_n(z)) \\
&= \lim_{n\to\infty} \sum_{k=1}^{n} (u_\alpha - u)(P_n(z)) \\
&= (u_\alpha - u)\Big(\lim_{n\to\infty} \sum_{k=1}^{n} P_n(z)\Big) \\
&= (u_\alpha - u)\Big(\sum_{n\geq 1} P_n(z)\Big).
\end{aligned}$$

Then $[T(u_\alpha)](z) \to [T(u)](z)$ for all $z \in U$. This implies that $v = T(u)$. Hence T has a closed graph.

Meanwhile, since F is Fréchet, by the research [7] [Theorem 13.4.2] we have

$\beta(F', F)_{\text{bor}} = \eta(F', F)$ on F', where $\eta(F', F)$ is the corresponding locally convex inductive limit topology on $F' = \bigcup_{U\in\mathscr{U}} F'_{U^\circ}$ with $\mathscr{U}$ consists of closed and absolutely convex sets in F. This implies that F'_{bor} is ultrabornological. On the other hand, because E is metrizable, we have

$$H(0_E) = \varinjlim_{n\to\infty} (H^\infty(V_n), \|\cdot\|_n)$$

where $(V_n)_{n\geq}$ is a countable fundamental neighbourhood system at $0 \in E$, and $\|\cdot\|_n$ is the norm on the Banach space $H^\infty(V_n)$ given by $\|f\|_n = \sup_{z\in V_n} |f(z)|$. Hence, by the closed graph theorem of Grothendieck [18] [Introduction, Theorem B], T is continuous.

Next, we shall show that there exists a neighbourhood V of $0 \in E$ such that $T : F'_{\text{bor}} \to H^\infty(V)$ is continuous linear.

We consider two cases: (a) E is Schwartz; (b') E is Banach and $F \in (LB_\infty)$.

The case (a): Since E is Schwartz, by [19] [Theorem 2 and Corollary 9], $H(0_E)$ has a continuous norm. Using Proposition 1.4 in [20] we deduce that there exists a neighbourhood V of $0 \in E$ such that $T : F'_{\text{bor}} \to H^\infty(V)$ is continuous linear.

The case (b'): Since E is Banach, it follows from [21] [Theorem 1] that $H(0_E) \in (\Omega)$. Then, because $(F'_{\text{bor}})'_\beta \in (LB_\infty)$, using Theorem 3.2 in [5] we deduce that there exists a neighbourhood V of $0 \in E$ such that $T : F'_{\text{bor}} \to H^\infty(V)$ is continuous linear.

Now we define the map $\widehat{f} : V \to F''_{\text{bor}}$ by the formula

$$[\widehat{f}(z)](u) = [T(u)](z), \quad z \in V,\ u \in F'_{\text{bor}}.$$

Since T is continuous and point evaluations on $H(V)_{\text{bor}}$ are continuous (see the research [9] [Proposition 3.19]) it follows that $\widehat{f}(z) \in F''_{\text{bor}}$ for all $z \in V$. Moreover, for each fixed $u \in F'_{\text{bor}}$ the mapping

$$z \in V \mapsto [T(u)](z)$$

is holomorphic, that is

$$\widehat{f} : V \to (F''_{\text{bor}}, \sigma(F''_{\text{bor}}, F'_{\text{bor}}))$$

is a continuous mapping. For all $a \in V, b \in E$ and all $u \in F'_{\text{bor}}$ the mapping

$$\{t \in \mathbb{C} :\ a + tb \in V\} \ni \lambda \mapsto u \circ \widehat{f}(a + \lambda b)$$

is a Gâteaux holomorphic mapping and hence

$$\widehat{f} : V \to (F''_{\text{bor}}, \sigma(F''_{\text{bor}}, F'_{\text{bor}}))$$

is holomorphic.

By the research [7] [8.13.2 and 8.13.3], F'_{bor} is a complete locally convex space. Hence by [22] [Theorem 4, p.210] applied to the complete space F'_{bor} we see that $(F''_{\text{bor}}, \sigma(F''_{\text{bor}}, F'_{\text{bor}}))$ and $(F'_{\text{bor}})'_\beta$ have the same bounded sets. An application of [23] [Proposition 13] shows that

$$\widehat{f} : V \to (F'_{\text{bor}})'_\beta$$

is holomorphic.

Let j denote the canonical injection from F into F''. If $z \in B := V \cap \{ta :\ t \in \mathbb{C}, a \in A\}$ and $\widehat{f}(z) \neq j(f(z))$ then there exists $u \in F'$ such that

$$\widehat{f}(z)(u) \neq j(f(z))(u) = u(f(z)).$$

This, however, contradicts the fact that for all $z \in B$ we have

$$\widehat{f}(z)(u) = [T(u)](z) = \sum_{n\geq 1} u(P_n)(z) = u(f(z)).$$

We now fix a non-zero $z \in B$. Then there exists a unique sequence in F'', $(a_{n,z})_{n=1}^\infty$, such that for all $\lambda \in \mathbb{C}$

$$\widehat{f}(\lambda z) = \sum_{n=0}^\infty a_{n,z}\lambda^n.$$

Since $\widehat{f}(0) = f(0) = a_{0,z}$ it follows that $a_{0,z} \in F$. Now suppose that $(a_{j,z})_{j=0}^n \subset F$. When $|\lambda| \leq 1$, $\widehat{f}(\lambda z) = f(\lambda z) \in F$. Hence, if $\lambda \in \mathbb{C}$, $0 < |\lambda| < 1$, then

$$\frac{\widehat{f}(\lambda z) - \sum_{j=0}^n a_{j,z}\lambda^j}{\lambda^{n+1}} = \sum_{j=n+1}^\infty a_{j,z}\lambda^{j-n-1} \in F.$$

Since F is complete we see, on letting λ tend to 0, that $a_{n+1,z} \in F$. By induction $a_{n,z} \in F$

https://doi.org/10.52111/qnjs.2024.18302

for all n and hence $\widehat{f}(\lambda z) \in F$ for all $\lambda \in \mathbb{C}$ and all $z \in B$. Since $\widehat{f}$ is continuous and F is a closed subspace of $(F'_{\text{bor}})'_\beta$ (see the research [24] [Lemma 2.1]) we have shown that $\widehat{f} : V \to F$ is holomorphic.

Hence, the series $\sum_{n\geq 1} P_n$ is convergent on V to f.

The proof of the case (a) is complete here. We continue the last step for the proof of the case (b) as follows:

(iii) *Step 3:* Let $\{U_n\}_{n\geq 1}$ be a decreasing basis of neighbourhoods of $0 \in E$. By $\mathcal{K}(E)$ we denote the family of all balanced convex compact subsets of E. By the case (b') in Step 2, for each $K \in \mathcal{K}(E)$ there exists $\varepsilon_K > 0$ such that f is uniformly convergent on $\varepsilon_K K$. Put

$$W = \bigcup_{K\in\mathcal{K}(E)} \varepsilon_K K.$$

Obviously, f is convergent on W. It remains to check that W is a neighbourhood of $0 \in E$. Assume the contrary, that W is not a neighbourhood of $0 \in E$. Then for each $n \geq 1$ there exists $x_n \in U_n \setminus W$. Put

$$K_0 := \overline{\text{conv}}\{0, x_1, x_2, \ldots\}.$$

By [25] [Corollary 6.5.4] we can find $K_1 \in \mathcal{K}(E)$, $K_0 \subset K_1$, such that K_0 is relatively compact in E_{K_1}. It implies that $x_n \to 0$ in E_{K_1}. Thus there exists $n_0 \geq 1$ such that for all $n \geq n_0$ we have $x_n \in \varepsilon_{K_1} K_1 \subset W$. This is incompatible with x_n being disjoint from W. □

4. ALEXANDER'S THEOREM FOR FRÉCHET-VALUED FORMAL POWER SERIES

We will present the proof of Theorem 1.2 in this section. Our work requires some extra results concerning to Vitali's theorem for a sequence of Fréchet-valued holomorphic functions.

Remark 4.1. In exactly the same way, Theorem 2.1 in the research [26] is true for the Fréchet-valued case.

Lemma 4.1. *Let E, F be Fréchet spaces, $D \subset E$ be an open set. Let $f : D \to F$ be a locally bounded function such that $\varphi \circ f$ is holomorphic for all $\varphi \in W \subset F'$, where W is separating. Then f is holomorphic.*

The proof of Lemma runs as in the proof of Theorem 3.1 in the research, [26] but here we use Vitali's theorem in the research [27] [Proposition 6.2] which states for a sequence of holomorphic functions on an open connected subset of a locally convex space.

Lemma 4.2. *Let D be a domain in a Fréchet space E and $f : D \to F$ be holomorphic, where F is a barrelled locally convex space. Assume that $D_0 = \{z \in D : f(z) \in G\}$ is not nowhere dense in D, where G is a closed subspace of F. Then $f(z) \in G$ for all $z \in D$.*

Proof. (i) We first consider the case $G = \{0\}$. On the contrary, suppose that $f(z^*) \neq 0$ for some $z^* \in D \setminus D_0$. By the Hahn-Banach theorem, we can find $\varphi \in F'$ such that $(\varphi \circ f)(z^*) \neq 0$. Let $z_0 \in (\text{int}\overline{D_0}) \cap D$ and let W be a balanced convex neighbourhood of $0 \in E$ such that $z_0 + W \subset \overline{D_0}$. Then by the continuity of f we deduce that $f = 0$ on $z_0 + W$. Hence, it follows from the identity theorem (see the research [27] [Proposition 6.6]) that $f = 0$ on D. This contradicts above our claim $(\varphi \circ f)(z^*) \neq 0$.

(ii) For the general case, consider the quotient space F/G and the holomorphic function $\omega \circ f : D \to F/G$ where $\omega : F \to F/G$ is the canonical map. Then $\omega \circ f \equiv 0$ on D_0. By the case (i), $\omega \circ f \equiv 0$ on D. This means that $f(z) \in G$ for all $z \in D$. □

Proposition 4.3. *Let E, F be Fréchet spaces and $D \subset E$ a domain. Assume that $(f_n)_{n\geq 1}$ is a locally bounded sequence of holomorphic functions on D with values in F. Then the following assertions are equivalent:*

(i) *The sequence* $(f_n)_{n\geq 1}$ *converges uniformly on all compact subsets of* D *to a holomorphic function* $f : D \to F$;

(ii) *The set* $D_0 = \{z \in D : \lim\limits_n f_n(z)$ *exists*$\}$ *is not nowhere dense in* D.

Proof. It suffices to prove the implication (ii) $\Rightarrow$ (i) because the case (i) $\Rightarrow$ (ii) is trivial. Define $\widetilde{f} : D \to \ell^\infty(\mathbb{N}, F)$ by $\widetilde{f}(z) = (f_n(z))_{n\geq 1}$, where $\ell^\infty(\mathbb{N}, F)$ is the Fréchet space with the topology induced by the system of seminorms

$$\|\!|x|\!\|_k = \|\!|(x_i)_{i\geq 1}|\!\|_k = \sup_i \|x_i\|_k,\ \forall k,$$

$\forall x = (x_i)_{i\geq 1} \in \ell^\infty(\mathbb{N}, F)$.

For each $k \in \mathbb{N}$ we denote $pr_k : \ell^\infty(\mathbb{N}, F) \to F$ is the k-th projection with $pr_k((w_i)_{i\in\mathbb{N}}) = w_k$. Obviously

$$W = \{\varphi \circ pr_k;\ \varphi \in F',\ k \in \mathbb{N}\} \subset \ell^\infty(\mathbb{N}, F)'$$

is separating and

$$\varphi \circ pr_k \circ \widetilde{f} = \varphi \circ pr_k \circ (f_n)_{n\geq 1} = \varphi \circ f_k$$

is holomorphic for every $k \geq 1$. Then by Lemma 4.1, $\widetilde{f}$ is holomorphic.

Since the space

$$G = \{(w_i)_{i\geq 1} \in \ell^\infty(\mathbb{N}, F) : \lim_{i\to\infty} w_i \text{ exists}\}$$

is closed, by the hypothesis, $\widetilde{f}(z) \in G$ for all $z \in D_0$. It follows from Lemma 4.2 that $\widetilde{f}(z) \in G$ for all $z \in D$. Thus $f(z) = \lim_{i\to\infty} f_i(z)$ exists for all $z \in D$. Note that $\Phi : G \to F$ given by $\Phi((y_i)_{i\in\mathbb{N}}) = \lim_{i\to\infty} y_i$ defines a bounded operator. Therefore $f = \Phi \circ \widetilde{f}$ is holomorphic.

Finally, in order to prove that $(f_i)_{i\geq 1}$ converges uniformly on compact sets in D to f, it suffices to show that $(f_i)_{i\geq 1}$ is locally uniformly convergent in D to f. Since $(f_i)_{i\geq 1}$ is locally bounded, by [27] [Proposition 6.1], $(f_i)_{i\geq 1}$ is equicontinuous at every $a \in D$. Let a be fixed point of D. Then for every balanced convex neighbourhood V of 0 in F there exists a neighbourhood U_a^1 of a in D such that

$$f_i(z) - f_i(a) \in 3^{-1}V,\ \forall z \in U_a^1,\ \forall i \geq 1. \quad (4.1)$$

Since $\lim\limits_{i\to\infty} f_i = f$ in D, we can find $i_0 \geq 1$ such that

$$f_i(a) - f(a) \in 3^{-1}V, \quad \forall i \geq i_0. \quad (4.2)$$

By the continuity of f, there exists a neighbourhood U_a^2 of a in D such that

$$f(a) - f(z) \in 3^{-1}V, \quad \forall z \in U_a^2. \quad (4.3)$$

From (4.1), (4.2) and (4.3), for all $z \in U_a = U_a^1 \cap U_a^2$ for all $i \geq i_0$ we have

$$f_i(z) - f(z) \in V. \quad (4.4)$$

The proof of the proposition is complete. □

We now can prove Theorem 1.2 as follows.

Proof of Theorem 1.2. As in the proof of Theorem 3.1, for each $n \geq 1$, define the continuous linear map $T_n : F'_{\text{bor}} \to H(0_{\mathbb{C}^N})$ given by

$$T_n(u) = u \circ f_n, \quad u \in F'_{\text{bor}}.$$

By Theorem 3.5 in the research, [3] the sequence $(T_n(u))_{n\geq 1}$ converges in $H(0_{\mathbb{C}^N})$ for every $u \in F'_{\text{bor}}$. Since F'_{bor} is barrelled (see the research [7] [13.4.2]) it follows that the sequence $(T_n)_{n\geq 1}$ is equicontinuous in $L(F'_{\text{bor}}, H(0_{\mathbb{C}^N}))$ equipped with the strong topology. As in the proof of Theorem 3.1, by Theorem 3.2 in [5] we deduce that there exists a neighbourhood U of $0 \in F'_{\text{bor}}$ such that

$$\bigcup_{n\geq 1} T_n(U)$$

is bounded in $H(0_{\mathbb{C}^N})$. By the regularity of $H(0_{\mathbb{C}^N})$, we can find $r \in (0, r_0)$ such that $\bigcup_{n\geq 1} T_n(U)$ is contained and bounded in $H^\infty(\Delta_N(r))$. This yields that $(f_n)_{n\geq 1}$ is contained and bounded in $H^\infty(\Delta_N(r), F)$. Since for each $z \in \Delta_N(r)$ the sequence $(f_n|_{\ell_z})_{n\geq 1}$ is convergent in $\Delta_1(r_0) \subset \ell_z$, by Remark 4.1,

https://doi.org/10.52111/qnjs.2024.18302

the sequence $(f_n(z))_{n\geq 1}$ is convergent for every $z \in \Delta_N(r)$. On the other hand, because $(f_n)_{n\geq 1}$ is bounded in $H^\infty(\Delta_N(r), F)$, by Proposition 4.3 it follows that the sequence $(f_n)_{n\geq 1}$ is convergent in $H(\Delta_N(r), F)$. □

Acknowledgments

This study is conducted within the framework of science and technology projects at institutional level of Quy Nhon University under the project code T2023.816.26. The author gratefully acknowledges the many helpful suggestions of Professor Thai Thuan Quang during the preparation of the paper.

REFERENCES

1. B. V. Shabat. *An introduction to complex analysis, part II, functions of several variables*, American Mathematical Society Providence, Rhode Island, 1992.
2. H. Alexander. Volumes of images of varieties in projective spaceand in Grassmannians, *Transactions of the American Mathematical Society*, **1974**, *189*, 237-249.
3. T. V. Long, L. T. Hung. Sequences of formal power series, *The Australian Journal of Mathematical Analysis and Applications*, **2017**, *452*(1), 218-225.
4. S. Dineen, R. Meise, D. Vogt. Characterization of nuclear Fréchet spaces in which every bounded set is polar, *Bulletin de la Société Mathématique de France*, **1984**, *112*, 41-68.
5. D. Vogt. Frecheträume zwischen denen jede stetige linear Abbildung beschraukt ist, *Journal für die Reine und Angewandte Mathematik*, **1983**, *345*, 182-200.
6. L. M. Hai, N. V. Khue. Hartogs spaces, spaces having the Forelli property and Hartogs holomorphic extension spaces, *Vietnam Journal of Mathematics*, **2005**, *33*(1), 43-53.
7. H. Jarchow. *Locally convex spaces*, Teubner, Suttgart, 1984.
8. N. V. Khue, L. M. Hai, B. Q. Hoan. Frechet-valued holomorphic functions on compact subsets in a normal complex space of dimension 2 and linear topological invariant (LB_∞), *Bulletin Mathématique de la Sociétédes Sciences Mathématiques de Roumanie*, **2005**, *48*(1), 45-63.
9. S. Dineen. *Complex analysis on infinite dimensional spaces*, Springer, New York, 1999.
10. Ph. Noverraz. *Pseudo-convexite, convexite polynomiale et domaines d'Holomorphie en dimension infinie*, North-Holland Publishing Company, Amsterdam-London, 1973.
11. M. Klimek. *Pluripotential theory*, Clarendon Press, Oxford, 1991.
12. J. Siciak. Extremal plurisubharmonic functions in $\mathbb{C}^n$, *Annales Polonici Mathematici*, **1982**, *39*, 175- 211.
13. E. Bedford, B. A. Taylor. A new capacity of plurisubharmonic functions, *Acta Mathematica*, **1982**, *149*, 1-40.
14. H. F. Hartogs. Zur theorie der analytischen funktionen mehreren unabhangiger veranderlichen, *Mathematische Annalen*, **1906**, *62*, 1-88.
15. P. Lelong. On a problem of M.A. Zorn, *Proceedings of the American Mathematical Society*, **1951**, *2*, 11-19.
16. A. Sathaye. Convergence sets of divergent power series, *Journal für die Reine und Angewandte Mathematik*, **1976**, *283*, 86 - 98.
17. N. Levenberg, R. Molzon. Convergent sets of a formal power series, *Mathematische Zeitschrift*, **1988**, *197*, 411-420.

18. A. Grothendieck. *Produits tensoriels topologiques et espaces nucléaires*, American Mathematical Society Providence, Rhode Island, 1966.

19. C. Boyd. Montel and reflexive preduals of spaces of holimorphic functions on Frechet spaces, *Studia Mathematica*, **1993**, *107*(3), 306-315.

20. J. Bonet, A. Galbis. The identity $L(E,F) = LB(E,F)$, tensor products and inductive limits, *Note di Matematica*, **1989**, *9*(2), 195-216.

21. N. V. Khue, P. T. Danh. Structure of spaces of germs of holomorphic functions, *Publicacions Matemàtiques*, **1997**, *41*(2), 467-480.

22. J. Horvath. *Topological vector spaces and distributions*, Addison-Wesley Publishing Company, Reading, Massachusetts, USA, 1966.

23. L.Nachbin. *Lecture notes in mathematics*, Springer, New York, 1974.

24. T. T. Quang, D. T. Vy, L. T. Hung, P. H. Bang. The Zorn property for holomorphic functions, *Annales Polonici Mathematici*, **2017**, *120*(2), 115-133.

25. H. Junek. *Locally convex spaces and operator ideals*, Leipzig, Teubner, 1983.

26. W. Arendt, N. Nikolski. Vector-valued holomorphic functions revisited, *Mathematische Zeitschrift*, **2000**, *234*, 777- 805.

27. J. Bochnak, J. Siciak. Analytic functions in topological vector spaces, *Studia Mathematica*, **1971**, *39*, 77- 112.

https://doi.org/10.52111/qnjs.2024.18302

TẠP CHÍ KHOA HỌC
TRƯỜNG ĐẠI HỌC QUY NHƠN

Tổng hợp CeO_2 và ứng dụng xử lý chất màu hữu cơ trong môi trường nước

Nguyễn Vũ Ngọc Mai[1,*], Ngô Thị Thanh Hiền[1], Nguyễn Thị Hà Chi[2], Đào Ngọc Nhiệm[2]

[1]Khoa Khoa học Tự nhiên, Trường Đại học Quy Nhơn, Việt Nam
[2]Viện Khoa học Vật liệu – Viện Hàn lâm Khoa học và Công nghệ Việt Nam, Việt Nam

Ngày nhận bài: 28/11/2023; Ngày sửa bài: 29/02/2024;
Ngày nhận đăng: 13/03/2024; Ngày xuất bản: 28/06/2024

TÓM TẮT

Nghiên cứu này tổng hợp vật liệu CeO_2 sử dụng hai tác nhân tạo gel là tartaric acid (A) và polyvinyl alcohol (P) bằng phương pháp đốt cháy. Các đặc trưng được sử dụng để phân tích mẫu tổng hợp được là DTA-TGA, XRD, BET, SEM. Vật liệu tổng hợp ở các điều kiện tối ưu được ứng dụng xử lí methylene blue (MB) trong môi trường nước. Kết quả phân tích MB cho thấy hiệu suất xử lí đạt gần 80% ở pH4, nồng độ đầu vào của chất ô nhiễm 10 ppm, hàm lượng chất xúc tác 1 g/L.

Từ khóa: *CeO_2, PVA, tartaric acid, MB.*

**Tác giả liên hệ chính.*
Email: nguyenvungocmai@qnu.edu.vn

QUY NHON UNIVERSITY
JOURNAL OF SCIENCE

Synthesis of CeO_2 and its application for treating organic dyes in water

Nguyen Vu Ngoc Mai[1,*], Ngo Thi Thanh Hien[1], Nguyen Thi Ha Chi[2], Dao Ngoc Nhiem[2]

[1]Faculty of Natural Sciences, Quy Nhon University, Vietnam
[2]Institute of Materials Science, Vietnam Academy of Science and Technology, Vietnam

Received: 28/11/2023; Revised: 29/02/2024;
Accepted: 13/03/2024; Published: 28/06/2024

ABSTRACT

The CeO_2 material was synthesized using two gelling agents: tartaric acid (A) and polyvinyl alcohol (P) through the combustion method. DTA-TGA, XRD, BET, and SEM methods were employed to analyze the characteristics of the synthesized material. The synthesized materials, prepared under optimal conditions, were utilized for the treatment of methylene blue (MB) in water. The efficiency achieved nearly 80% at pH4 with an input concentration of the pollutant at 10 ppm and a catalyst concentration of 1 g/L.

Keywords: *CeO_2, PVA, tartaric acid, methylene blue.*

1. INTRODUCTION

Currently, environmental pollution poses a significant global challenge, including in Vietnam. Untreated or improperly treated waste released into the environment pollutes the soil, water, and air, directly impacting human life. Various methods are being applied and researched to treat pollutants, each with its own set of advantages and disadvantages.

Recently, photocatalytic method using CeO_2 catalyst has received research attention. Research results showed the effectiveness of CeO_2 in treating pollutants that are difficult to biodegrade[1,2] as well as pigments.[3,4] The advantages of CeO_2 are manifested in its structure. According to research,[5] in the unit structure of CeO_2, the cation Ce^{4+} was easily replaced by Ce^{3+}. To compensate for the charge, the part of the oxygen elements were lost and created oxygen vacancies. Therefore, CeO_2 was converted to the form CeO_{2-n}. These oxygen vacancies were the reason for their effectiveness in catalytic reactions.

CeO_2 material was synthesized by many different methods such as hydrothermal,[6] sol-gel,[7] combustion method[8]...or a combination of methods. The combustion method offers the advantage of simplicity and the capability to synthesize a large quantity of material. In this study, two gelling agents, PVA and tartaric acid, were combined. The addition of tartaric acid to the reaction mixture enhanced its complexation ability, provided additional heat, reduced the concentration of PVA, and lowered the synthesis temperature of the material.

**Corresponding author.*
Email: nguyenvungocmai@qnu.edu.vn

https://doi.org/10.52111/qnjs.2024.18303

2. EXPERIMENT

2.1. Material synthesis process

Oxide nanoparticles of CeO_2 were synthesized by the combustion method. The gelling agents were dissolved in water with salt solutions of Ce^{3+} in appropriate molar ratios. The solution was stirred and heated until transparent gel was formed. The formation gel had high viscosity and was dried for 2 hours at 110 ^oC. Finally, it formed a puffy, spongy mass. Material products were obtained after calcinating at different temperatures. pH buffers were used to investigate desire pH. The chemicals used in this study were analytical quality.

2.2. Photocatalytic process

Research investigated the degradation of MB via photocatalytic processes employing CeO_2 nanoparticle oxides. Initially, a solution containing a specified concentration of the contaminant and catalyst was introduced into the reactor system (250 mL). Following this, the suspension was stirred in darkness for 60 minutes to establish an adsorption/desorption equilibrium before irradiation. After that, the mixture was lit by LED light with power 220 V, 30 W with different times. At specific time points, approximately 5 mL of the mixture was withdrawn, centrifuged, and subsequently filtered to remove the residual catalyst particulates for analysis. The concentration of MB was determined using UV-Vis spectroscopy (CE-2011) at a wavelength of 663 nm.

3. RESULTS AND DISCUSSION

3.1. Effect of calcination temperature

Different thermal analysis method was used to investigate calcination temperature of dried sample synthesized gelation temperature of 80 ^0C; pH4; Ce/AP ratio = 1/3; AP ratio = 1/1. The results were shown in Figure 1.

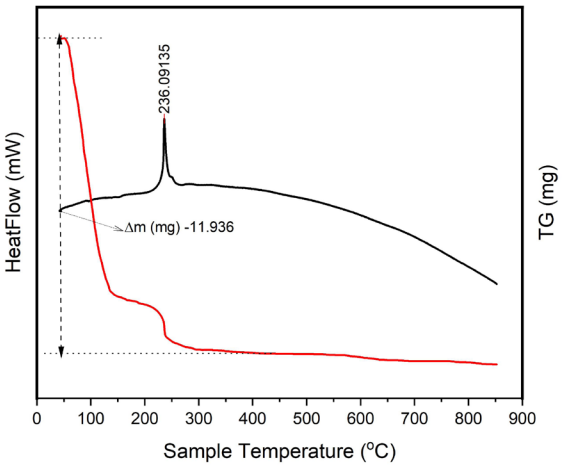

Figure 1. DTA – TGA of gel sample.

Figure 1 depicts a rapid weight loss observed within the temperature range of 30 to 300 ^0C, attributed to both dehydration and decomposition of PVA and tartaric acid within the sample. This phenomenon aligns with the distinct exothermic peak recorded at 236.09 ^0C on the DTA curve. Subsequently, minimal mass variation was noted above the TGA curve, indicative of the formation of the pure product.

To examine the formation of CeO_2 material, the sample underwent calcination at various temperatures. The outcomes are illustrated in Figure 2.

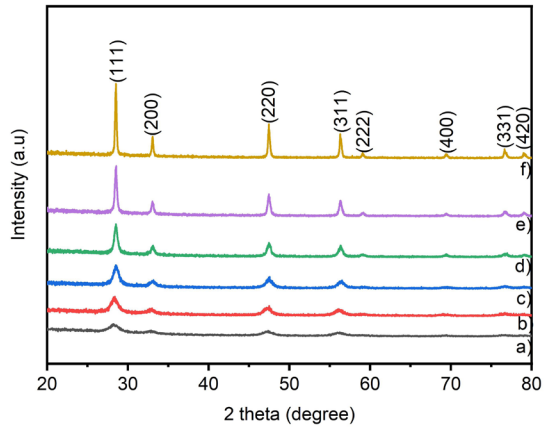

Figure 2. XRD diagrams of samples at different temperatures a) 300 ^0C; b) 400 ^0C; c) 450 ^0C; d) 500 ^0C; e) 600 ^0C; f) 700 ^0C.

The peaks located at 2θ = 28.99; 33.39; 47.91; 56.75; 59.1; 69.6; 76.5 and 79.47 correspond to the (111), (200), (220), (311),

(222), (400), (331), and (420) crystal planes of CeO_2, respectively, according to JCPDS card: 34-0394.[9] These peaks began to appear at low temperatures of 300 ^{0}C, and the peaks formed more clearly when sample was calcined at higher temperatures. Here the calcination temperature of 400 ^{0}C was chosen for further studies.

3.2. Effect of pH

After choosing the appropriate calcination temperature, the sample was surveyed to select the optimal pH for the synthesis process. Sample was kept at conditions: gelation temperature 80 ^{0}C; Ce/AP ratio = 1/3; AP ratio = 1/1; calcinating temperature 400 ^{0}C and pH values were changed by pH2, pH3, pH4. The results were shown in Figure 3.

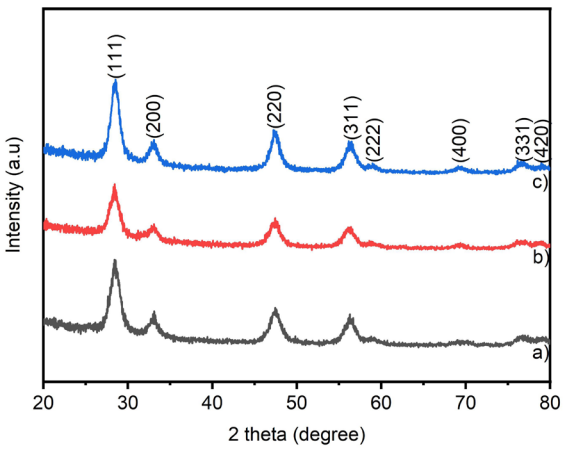

Figure 3. XRD diagrams of samples at a) pH2; b) pH3; c) pH4.

Figure 3 distinctly displays the formation of diffraction peaks specific to CeO_2. The findings indicate that pH did not significantly influence the phase formation process of CeO_2 oxide in this study. However, if the pH is low (pH2, pH3), it can break the polymer chains of PVA, reducing the uniform dispersion of metal cations in the network. The appropriate pH here is pH3, pH4. In the next study, pH4 was chosen.

3.3. Effect of Ce/AP ratio

The ratio of metal and the gelling agent mixture were studied. The sample was synthesized at a gelation temperature of 80 ^{0}C; AP ratio = 1/1; calcinating temperature 400 ^{0}C; pH4; and Ce/AP ratios were changed at values of 9/1; 3/1; 1/1; 1/3; 1/9. Figure 4 showed the results of XRD diagrams of the synthesized samples.

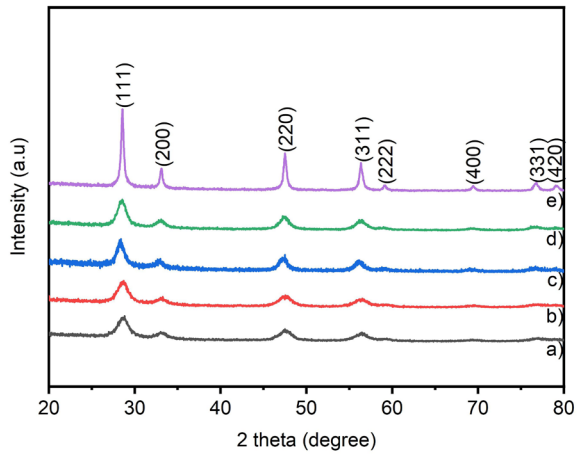

Figure 4. XRD diagrams of samples with different Ce/AP ratios a) Ce/AP = 9/1; b) Ce/AP = 3/1; c) Ce/AP = 1/1; d) Ce/AP =1/3; e) Ce/AP = 1/9.

At ratios of Ce/AP = 9/1; Ce/AP = 3/1; Ce/AP = 1/1 of the amount of agent used to form complexes with metal ions were not enough, resulting gels exhibited poor viscosity. When forming gels at Ce/AP = 1/3 and 1/9, it ensured the appropriate amount of gel-forming agent, leading to high viscosity gels. Upon thermal treatment, the products showed increased porosity and more uniform particle sizes. However, as shown in Figure 4, at the Ce/AP = 1/9, the peaks formed were higher and sharper compared to the Ce/AP = 1/3. This may indicate an increase in the crystal size of the obtained material. Therefore, the Ce/AP = 1/3 was chosen for further studies.

3.4. Effect of gel formation temperature

To investigate gel formation temperature, the sample was synthesized at conditions Ce/AP ratio = 1/3; AP ratio = 1/1; calcinating temperature 400 ^{0}C; pH4, and gel formation temperatures were changed at 40 ^{0}C, 60 ^{0}C, 80 ^{0}C, 100 ^{0}C. The results were shown in Figure 5.

https://doi.org/10.52111/qnjs.2024.18303

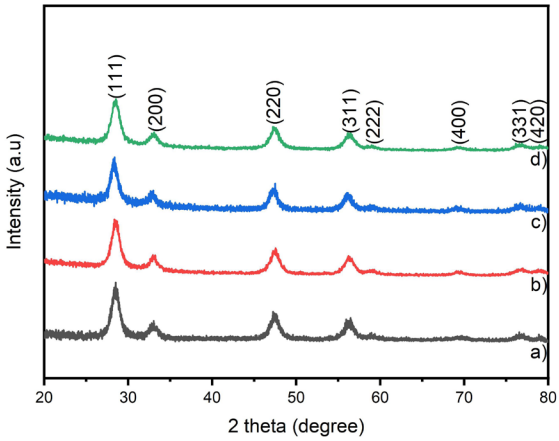

Figure 5. XRD diagrams of sample at different gel formation temperatures a) 40 ^{0}C, b) 60 ^{0}C, c) 80 ^{0}C, d) 100 ^{0}C.

The synthesis time for sample preparation was observed to be prolonged, taking 8 hours at 40 ^{0}C and 4 hours at 60 ^{0}C. Surprisingly, at 100 ^{0}C, although the synthesis duration was shorter (an hour), the characteristic peaks of CeO_2 were distinctly evident in the XRD pattern. However, significant noise in the background suggested potential instability in the product. Conversely, at 80 ^{0}C, the synthesis duration of 2 hours was sufficient for uniform distribution of metal ions within the complexing agent's network, resulting in clear and well-defined peaks of CeO_2 in the XRD pattern. Consequently, a temperature of 80 ^{0}C was selected for synthesizing the desired sample.

3.5. Material characteristic after choosing optimum conditions

The CeO_2 oxide successfully synthesized under the studied conditions was employed for decomposing pollutants via a photocatalytic process. This process was notably influenced by factors such as grain size, material surface area, and more. The material characterization results are presented in Figure 6 and Table 1.

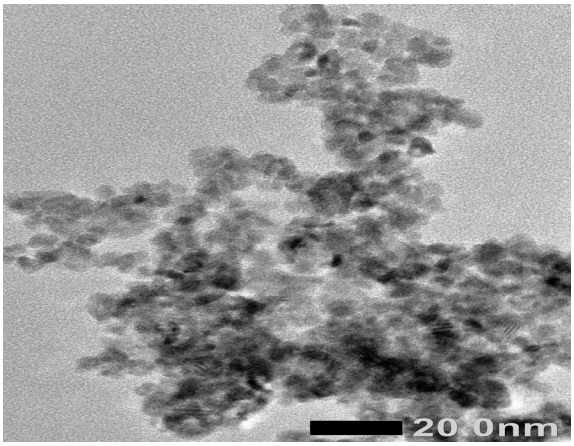

Figure 6. TEM image of CeO_2.

Figure 6 showed that the oxide nanoparticles of CeO_2 were spherical with an average size of about 10 nm. When compared with similar studies[10,11] that used only alone gelling agent the results were shown in Table 1.

Table 1. Comparision of CeO_2 material formed by using gel agents PVA, AT and mixture of PVA and AT.

Gel agent	Calcination temperature (^{0}C)	BET (m^2/g)	References
PVA	180	35.0	[10]
AT	600	38.57	[11]
AP	400	72.97	This study

The calcination temperature of the sample using the AP gelling agent mixture was lower by 200 ^{0}C compared to the sample using AT alone. Additionally, the specific surface area of the sample using the AP gelling agent mixture was nearly double that of the sample using the gelling agent alone. This demonstrates the advantage of employing a mixture of gelling agents, PVA and AT. The combination enhanced the ability to form complexes with AT and achieve even distribution on the structural net of PVA. The even distribution of heat reduced the required heating temperature, resulting in a final product with a larger specific surface area, thereby creating favorable conditions for the decomposition of pollutants. Figure 7 shows the N_2 adsorption–desorption isotherms and the pore size distribution plot of the CeO_2 samples.

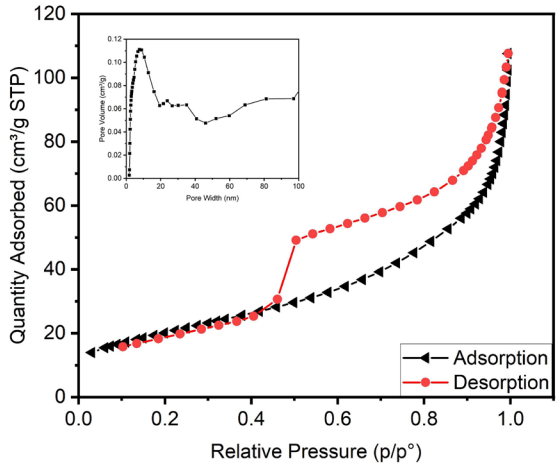

Figure 7. Nitrogen adsorption–desorption isotherm and the pore size distribution plot for the synthesized CeO_2 sample.

Figure 7 shows that the adsorption and desorption isotherms of the CeO_2 material samples exhibit type IV (according to the IUPAC classification), characteristic of mesoporous structures. The average pore diameter was calculated using the BJH method to be 9.7 nm.

3.6. Photocatalytic process to decompose organic pigment of CeO_2 material

3.6.1. Effect off catalyst concentration

The material was continued to research on the influence of catalyst content on the MB decomposition process. The initial concentration of the pollutant was 10 ppm, pH 4, the catalyst content was changed at values of 0.25 g/L, 0.5 g/L, 1 g/L, 1.5 g/L. The results were shown in Figure 8.

The results demonstrated that as the catalyst content increased, the efficiency of MB treatment also increased over time, reaching its peak at a catalyst content of 1.0 g/L after 7 hours of treatment (80%). However, with a further increase in the catalyst content to 1.5 g/L, the efficiency of MB treatment decreased. This could be attributed to the material's black color, which potentially reduced the amount of light reaching the material, thereby affecting the efficiency of the pollutant treatment process.

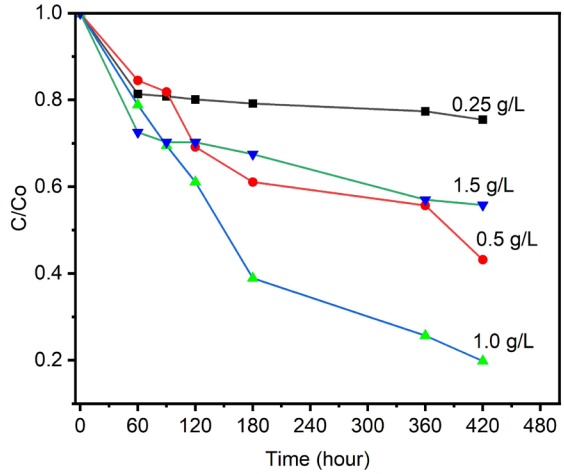

Figure 8. Effect of catalyst content to MB decomposistion over time.

3.6.2. Effect of initial concentration

The initial pollutant concentration was changed at 5 ppm, 10 ppm, 15 ppm at pH4, catalyst content 1 g/L. The results were shown in Figure 9.

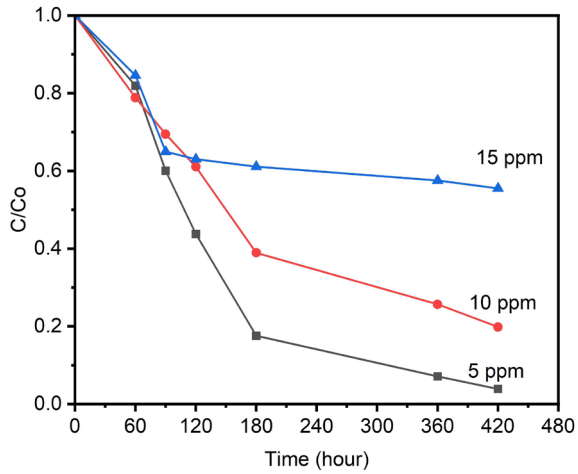

Figure 9. Effect of initial concentration to MB decomposition over time.

The initial concentration of the pollutant greatly affected the pollutant treatment process. MB concentration was increased; therefore, it led to an increase in the amount of pollutants in the reaction mixture. With the same catalytic content and a certain number of active sites, the amount of MB adsorbed on these active sites were greater. Therefore, the number of active sites were not enough to decompose this amount of pollutant. The efficiency of decomposing pollutants decreased.

https://doi.org/10.52111/qnjs.2024.18303

During photocatalysis, electron/hole pairs are formed under appropriate light conditions. Similar to the study by Le Thi Thanh Tuyen,[9] under UV light irradiation, these electrons further react with dissolved oxygen to generate superoxide radical anions ($O_2^{\bullet-}$), while h^+ in the valence band reacts with adsorbed water and produces more hydroxyl radicals (•OH). These strong oxidizing radicals are reactive species which are mainly responsible for degradation of MB.

4. CONCLUSION

Oxide nanoparticles of CeO_2 were successfully synthesized under optimized conditions: calcination temperature at 400 ^{0}C, pH4, Ce/AP = 1/3, AP = 1/1, and gelation temperature at 80 ^{0}C. The resulting nanoparticles exhibited a spherical shape with an average particle size of approximately 10 nm and a surface area of 72.97 m^2/g, nearly doubling that achieved when using either the gelling agent PVA (35 m^2/g) or AT (38.57 m^2/g) individually.

The photocatalytic process utilizing these CeO_2 nanoparticles demonstrated an efficiency of 80 % in treating MB under conditions of pH4, initial MB concentration of 10 ppm, catalyst content at 1 g/L, and a reaction duration of 7 hours.

Acknowledgments

This research is conducted within the framework of science and technology projects at institutional level of Quy Nhon University under the project code T2023.798.08.

REFERENCES

1. M. Aslam, M. T. Qamar, M. T. Soomro, I. M. I. Ismail, N. Salah, T. Almeelbi, M. A. Gondal, A. Hmeed. The effect of sunlight induced surface defects on the photocatalytic activity of nanosized CeO_2 for the degradation of phenol and its derivatives, *Applied Catalysis B: Environmental*, **2016**, *180*, 391-402.
2. K. Yea, Y. Lib, H. Yanga, M. Lia, Y. Huang, S. Zhang, H. Ji. An ultrathin carbon layer activated CeO_2 heterojunction nanorods for photocatalytic degradation of organic pollutants, *Applied Catalysis B: Environmental*, **2019**, *259,* 1-8.
3. L. H. Trinh, N. D. Cuong, D. D. Trung, N. V. Hieu. Synthesis and characterization of hierarchical CeO_2 spherical nanoparticles for photocatalytic degradation of methylene blue, *VNU Journal of Science: Mathematics – Physics*, **2021**, *4*, 76-85.
4. R. Bakkiyaraj, M. Balakrishnan. Physical, optical and photochemical properties of CeO_2 nanoparticles synthesized by solution combustion method, *Journal of Advanced Physics*, **2017**, *6*(1), 41-47.
5. N. T. H. Tram, N. D. M. Tuan. Synthesis of CeO_2 catalyst for complete oxidation of toluene and isopropanol, *The University of Danang - Journal of Science and Technology*, **2021**, *19*(3), 29-32.
6. A. I. Y. Tok, F. Y. C. Boey, Z. Dong, X. L. Sun. Hydrothermal synthesis of CeO_2 nanoparticles, *Journal of Materials Processing Technology*, **2007**, *190*, 217-222.
7. P. Periyat, F. Laffir, S. A. M. Tofail, E. Magner. A facile aqueous sol–gel method for high surface area nanocrystalline CeO_2, *RSC Advances*, **2011**, *1*, 1794-1798.
8. T. Mokkelbost, I. Kaus, T. Grande, M. A. Einarsrud. Combustion synthesis and characterization of nanocrystalline CeO_2-based powders, *Chemistry of Materials*, **2004**, *16*(25), 5489-5494.
9. L. T. T. Tuyen, D. Q. Khieu, H. T. Long, D. T. Quang, C. T. L. Trang, T. T. Hoa, N. D. Cuong. Monodisperse uniform CeO_2 nanoparticles: controlled synthesis and photocatalytic property, *Journal of Nanomaterials*, **2016**, *2016*, 8682747.
10. N. G. Hung, L. M. Dai, V. Q. Mai, D. N. Nhiem. Low temperature synthesis of nanostructured cerium dioxide by auto combustion process of polyvinyl alcohol-cerium nitrate gel, *Journal of Chemistry*, **2004**, *42*, 444-448.
11. V. Q. Mai, T. T. C. Phuong. Synthesis of ultrafine CeO_2 via sol-gel method from cerium (IV) nitrate and tartaric acid, *Hue University Journal of Science*, **2008**, *48*, 119-124.

TẠP CHÍ KHOA HỌC
TRƯỜNG ĐẠI HỌC QUY NHƠN

Tổng hợp vật liệu composite g-C_3N_4/ZnO tăng cường hoạt tính quang xúc tác dưới ánh sáng nhìn thấy

Phan Thị Thùy Trang[1,*], Đặng Trung Hậu[2], Nguyễn Vũ Diệu Linh[2], Nguyễn Văn Thưởng[2], Nguyễn Hồ Duy[2], Nguyễn Lương Khương An[2], Mai Thị Tường Vy[3], Nguyễn Thị Lan[1,*]

[1]Khoa Khoa học Tự nhiên, Trường Đại học Quy Nhơn, Việt Nam
[2]Khoa Sư Phạm, Trường Đại học Quy Nhơn, Việt Nam
[3]Phòng Hành chính - Tổng hợp, Trường Đại học Quy Nhơn, Việt Nam

Ngày nhận bài: 03/12/2023; Ngày sửa bài: 07/03/2024;
Ngày nhận đăng: 25/03/2024; Ngày xuất bản: 28/06/2024

TÓM TẮT

Vật liệu composite ZnO/g-C_3N_4 đã được tổng hợp thành công bằng phương pháp nung đơn giản từ các tiền chất g-C_3N_4 và zinc acetate hexahydrate. Hình thái, độ kết tinh, thuộc tính hình học và liên kết hóa học của vật liệu được đặc trưng bằng các kỹ thuật phân tích khác nhau như hiển vi điện tử quét (SEM), nhiễu xạ tia X (XRD), phổ phản xạ khuếch tán tử ngoại khả kiến (UV-Vis DRS), phổ hồng ngoại (FT-IR). Vật liệu được đánh giá hiệu quả quang xúc tác qua phản ứng phân hủy dung dịch rhodamine B (RhB) dưới ánh sáng nhìn thấy. Kết quả cho thấy hoạt tính quang xúc tác của vật liệu composite phân hủy dung dịch RhB cao hơn các vật liệu đơn ZnO, g-C_3N_4 với hằng số tốc độ phản ứng phân hủy là 0.0243 phút^{-1}, gấp hơn hai lần so với g-C_3N_4 tinh khiết (0.0091 phút^{-1}).

Từ khóa: *g-C_3N_4, ZnO, composite, hoạt tính quang xúc tác, rhodamine B.*

**Tác giả liên hệ chính.*
Email: nguyenthilan@qnu.edu.vn, phanthithuytrang@qnu.edu.vn

https://doi.org/10.52111/qnjs.2024.18304

QUY NHON UNIVERSITY
JOURNAL OF SCIENCE

Synthesis of g-C_3N_4/ZnO composite with enhanced visible light photocatalytic activity

Phan Thi Thuy Trang[1,*], Dang Trung Hau[2], Nguyen Vu Dieu Linh[2], Nguyen Van Thuong[2], Nguyen Ho Duy[2], Nguyen Luong Khuong An[2], Mai Thi Tuong Vy[3], Nguyen Thi Lan[1,*]

[1]Faculty of Natural Sciences, Quy Nhon University, Vietnam
[2]Faculty of Education, Quy Nhon University, Vietnam
[3]Administrative - General Office, Quy Nhon University, Vietnam

Received: 03/12/2023; Revised: 07/03/2024;
Accepted: 25/03/2024; Published: 28/06/2024

ABSTRACT

ZnO/g-C_3N_4 composite material was successfully synthesized using a facile calcination method with g-C_3N_4 and zinc acetate hexahydrate as the precursors. The morphology, crystallinity, optical properties, and chemical bond characteristics of the synthesized composite were characterized by using various analytical techniques such as scanning electron microscopy (SEM), Fourier-transform infrared (FTIR) spectroscopy, X-ray powder diffraction (XRD), ultraviolet-visible diffuse reflectance spectroscopy (UV-Vis DRS). The material's photocatalytic performance was evaluated through the decomposition of rhodamine B (RhB) solution under visible light. The results show that the photocatalytic properties of composite materials decomposing RhB dye solution are higher than those of single materials ZnO, g-C_3N_4 with a decomposition reaction rate constant of 0.0243 min^{-1}, more than twice as fast compared to pure g-C_3N_4 (0.0091 min^{-1}).

Keywords: *g-C_3N_4, ZnO, composite, photocatalytic activity, rhodamine B.*

1. INTRODUCTION

Along with economic development nowadays, the problem of environmental pollution is becoming increasingly serious. Therefore, effectively treating ecological decay is a challenging problem at the global level. Environmental treatment methods have been widely researched and have achieved many good results, including popular methods such as physics, chemistry, and biology. Recently, an attractive method for scientists to treat difficult-to-decompose organic substances is using semiconductor photocatalytic materials. Among the semiconductors published to date, metal oxides are the most studied due to their chemical and photochemical stability, low toxicity, and low cost.[1] Among the oxides, TiO_2 and ZnO are of most interest.[2] ZnO is a potential candidate for photocatalytic reactions due to its high photocatalytic activity, environmental compatibility, and relatively low cost and is therefore widely used in wastewater treatment.[3,4]

Zinc oxide (ZnO) is a widely researched and widely used semiconductor in photocatalysis. However, ZnO has a wide band gap energy (about

**Corresponding author.*
Email: nguyenthilan@qnu.edu.vn, phanthithuytrang@qnu.edu.vn

https://doi.org/10.52111/qnjs.2024.18304

3.37 eV), so it is less active in the visible light region.[5] It is an exciting idea to prepare a mix with two photocatalysts by appropriate matching band-level sites to reduce the electron−hole pair recombination.[6]

Recently, g-C_3N_4 material, a polymer organic semiconductor with a graphitic-like structure, can absorb visible light (the band gap energy of about 2.7 eV), taking many interest researchers due to its wide range of applications. However, the fast recombination rate of photoinduced electron-hole pair for this material leads to its low photoefficiency. This is a drawback when using it in individual status. Therefore, many attempts to enhance the photocatalytic performance of g-C_3N_4 by modifying it with other elements have been made.[7,8]

In this study, the ZnO/g-C_3N_4 composite was synthesized by a simple calcination method, and its photocatalytic efficiency was determined through the degradation of RhB under visible light.

2. EXPERIMENTAL

2.1. Material synthesis

Chemicals

All the chemicals for materials synthesis, including *zinc acetate* dehydrate $Zn(CH_3COO)_2.2H_2O$ (99.5%), urea ($CO(NH_2)_2$, ≥ 99%), rhodamine B ($C_{28}H_{31}ClN_2O_3$) were purchased from Merck.

Synthesis

The pure g-C_3N_4 was prepared by heating urea in an alumina crucible covered by an alumina sealed with aluminum foil at 550 °C in the Argon gas for an hour with a temperature ramping of 10 °C·min^{-1}. The obtained solid product was re-grounded and denoted as g-C_3N_4.

The g-C_3N_4/ZnO was synthesized through the calcination facile method. Firstly, 100 mg of g-C_3N_4 was a mixture with 200 mg of zinc acetate dehydrate $Zn(CH_3COO)_2.2H_2O$. Next, the mixture was ground finely and calcined in the air at 350 °C for 1 hour. The solid was filtered, washed, and dried at 80 °C for 24 hours to obtain the composite product ZnO/g-C_3N_4 (denoted as ZCN). ZnO was also synthesized similarly to the above conditions but without g-C_3N_4 (marked as ZnO).

2.2. Characterization

Powder X-ray diffraction (PXRD) patterns were acquired using a Bruker diffractometer (D/max 2200) with Ni-filtered Cu Ka radiation (k = 1.5418 Å), power 40 kV, current 40 mA. Scanning angle from 10 to 80°. The Fourier-transform infrared (FT-IR) spectroscopy was carried out on an IRAffinity-1S spectrometer (Shimadzu) with wavenumbers ranging from 400 to 4000 cm^{-1}. The composition of the element was determined by EDS spectroscopy. UV-Vis-DRS spectra of material samples were determined on a Jasco-V770 machine with wavelengths from 200 - 800 nm. The morphology and size of the synthesized samples were characterized by scanning electron microscopy (SEM, JEOL JSM-600F).

2.3. Photocatalytic properties

Rhodamine B (RhB, $C_{28}H_{31}ClN_2O_3$) was selected as an organic pollutant to evaluate photocatalytic activity. To 100 mL of 10 mg/L RhBsolution, 0.05 g of prepared sample was dispersed under stirring, and the solution was kept in a dark condition for 30 min. Then, the solution was irradiated by visible light using a 30 W LED lamp source. RhB degradation was monitored by taking suspension at irradiation time intervals of 20 min. Each suspension was centrifuged to separate the catalyst from the RhB solution. Subsequently, the degradation rate was calculated as a function of irradiation time from the change in absorbance at a wavelength of 553 nm as measured using a UV–Vis spectrophotometer (Jenway 6800).

3. RESULTS AND DISCUSSION

3.1. Material characteristics

The X-ray diffraction patterns of ZnO, g-C_3N_4, and ZCN composite are shown in Figure 1. The

patterns show that the photocatalysts are well crystallized, the pure g-C_3N_4 sample has two distinct peaks at 12.87° and 27.69°, which are indexed for graphitic materials as the (100) and (002).[9] The peak at 12.87° represents stacking of aromatic units corresponding to the interplanar distance of 6.82 Å. The strong peak at 27.69° is interlayer packing of aromatic tri-s-triazine with a stacking distance of 3.22 Å.[10] Meanwhile, the diffraction peaks at 2θ = 31.76°, 34.44°, 36.26°, 47.56°, 56.64°, 62.94° và 68.19° in XRD patterns of ZnO, corresponding to the (100), (002), (101), (102), (110), (103) and (112).[11] The XRD peaks of the pure ZnO sample agree with the hexagonal wurtzite structure (JCPDS No. 001-1136). The locus and shapes of characteristic peaks of ZCN are unchanged compared with those of pure ZnO. This demonstrated that modification with g-C_3N_4 does not affect ZnO's lattice structure, which is suitable for photocatalytic properties of as-prepared hybrid photocatalysts. As for a combination, the ZCN composites show the X-ray patterns analogous to the X-ray patterns of the components. The diffraction peaks of both ZnO and g-C_3N_4 phases are observable.

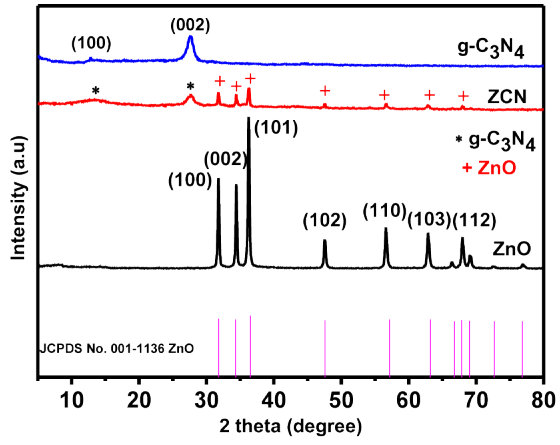

Figure 1. XRD patterns of g-C_3N_4, ZnO, and ZCN.

The bond structure of ZnO, g-C_3N_4, and ZCN composite were analyzed by FT-IR measurement. Figure 2 shows that the spectrum of g-C_3N_4 has found some strong bands in the 1616 -1200 cm^{-1} range, corresponding to typical stretching vibrations of C-N, C = N heterocycles.[12] The peak at 800 cm^{-1} was assigned to the s-triazine ring vibrations. While the peaks at 1616, 1560, 1461, and 1405 cm^{-1} were ascribed to stretching vibrations of heptazine-desired repeating units. The peak at 1313 and 1232 cm^{-1} belonged to the stretching vibration of connected trigonal units of C-N(-C)-C of bridging C-NH-C (partial condensation).[13] Meanwhile, the broad absorption band 3300 - 3000 cm^{-1} and a small peak at 891 cm^{-1} can be ascribed to the N-H stretching vibrations and bend vibration, respectively.[14-17] With the ZnO sample, there was a Zn-O bond vibration band at 550-450 cm^{-1}.[18] In general, all the characteristic peaks of ZnO and g-C_3N_4 appeared in the spectra of ZCN. Combined with the XRD and FT-IR analysis, it reconfirmed the successful synthesis of the ZCN composite. The result showed a strong interaction between g-C_3N_4 and ZnO semiconductors.

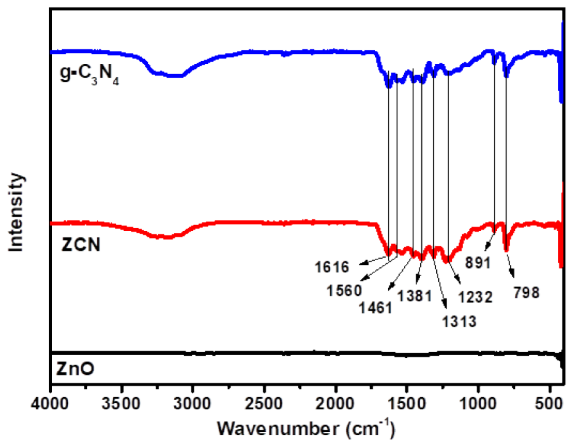

Figure 2. IR spectra of ZnO, g-C_3N_4 and ZCN.

The morphologies of ZnO, g-C_3N_4, and ZCN samples are indicated through SEM images in Figure 3.

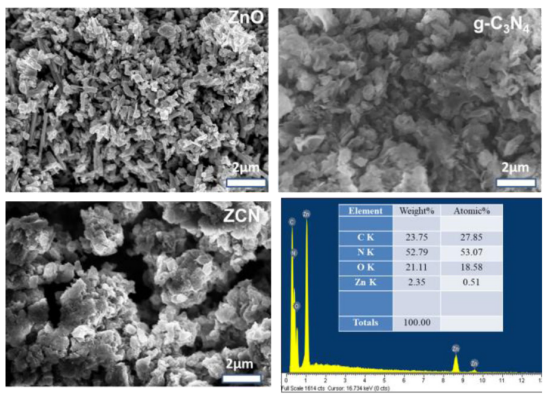

Figure 3. FE-SEM images of ZnO, g-C_3N_4, ZCN, and EDS image of ZCN.

https://doi.org/10.52111/qnjs.2024.18304

The results show that a typical multi-layered structure of graphitic carbon nitride corresponds to the in-plane structural packing pattern of tri-s -triazine building blocks. Figure 3 indicates that the ZCN material has micropores with large diameters. SEM image of ZnO in uneven sheet form, flat surface. After combining with g-C_3N_4, the morphology of ZCN changed significantly. This change in morphology can be ascribed to the surface deposition of g-C_3N_4 on the ZnO. The thin nanosheets encircled ZnO can be ascribed to g-C_3N_4 nanosheets. The ZnO core was uniformly beset with thin g-C_3N_4 flakes.[14] These results further confirm the successful formation of the heterostructure of ZCN. Figure 3 shows enough presence of elements Zn, O, C, and N in a composite sample of the EDS spectrum.

UV-vis diffuse reflectance spectra investigated optical absorptions of g-C_3N_4, ZnO, and ZCN (Figure 4).

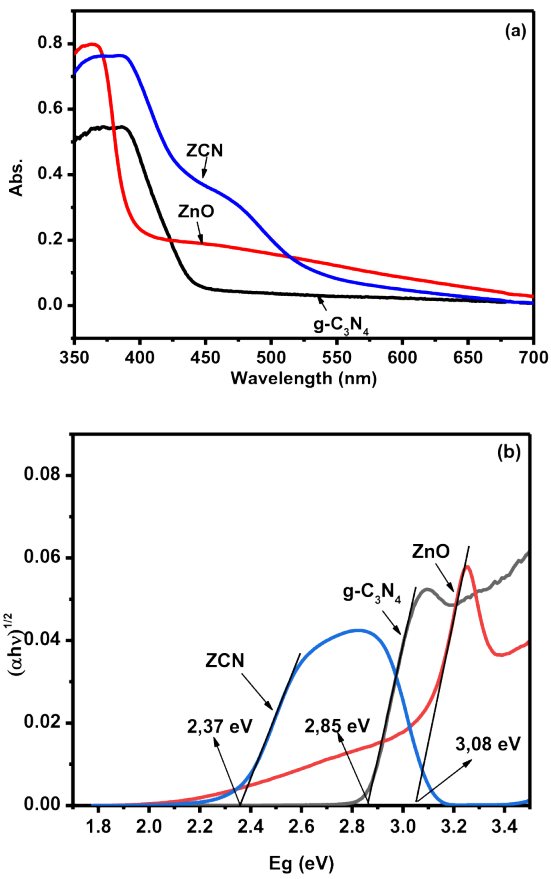

Figure 4. UV-Vis-DRS (a) and band gap of ZnO, g-C_3N_4, and ZCN (b).

The results show a clear fundamental absorption edge of ZnO at 395 nm, and the band gap energy is determined to be 3.08 eV. Meanwhile, the main absorption edge of pure g-C_3N_4 occurs at a wavelength of about 445 nm and a band gap energy of 2.85 eV. As expected, compared with pure ZnO, the ZCN photocatalyst shows the same absorption edge, but the absorption extends to the visible light in the presence of g-C_3N_4. This result can be expected to be that the photocatalytic reaction of ZnO is improved under visible light irradiation when g-C_3N_4 is introduced into ZnO and leads to charge transfer between g-C_3N_4 and the valence band of ZnO.

3.2. Photocatalytic properties of materials

The photocatalytic activity of the decomposition of RhB solution (10 mg/L) by LED lamp 30 W of materials is shown in Figure 5.

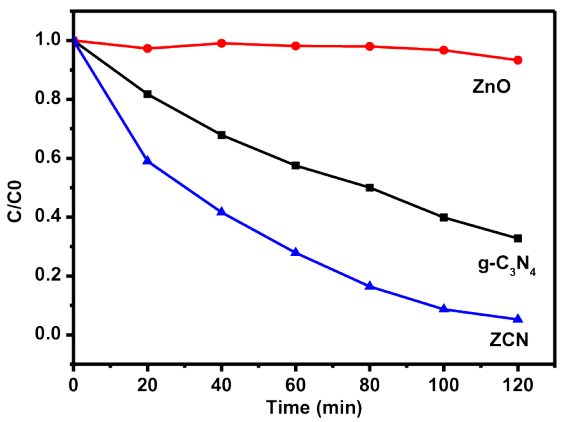

Figure 5. Decolorization kinetics of RhB over ZnO, g-C_3N_4, and ZCN under visible light irradiation (conditions: $m_{catalyst}$ = 0.05 g; concentration of RhB = 10 mg/L; adsorption time = 30 min).

Before evaluating the catalytic activity, the material samples were adsorbed in the dark for 30 minutes to reach adsorption/desorption equilibrium. Figure 5 shows that the ZCN sample exhibits higher photocatalytic activity to decompose RhB than the single ZnO and g-C_3N_4 after 120 minutes of illumination. Specifically, the photocatalytic efficiency of samples ZnO, g-C_3N_4, and ZCN is 6.68%, 67.27%, and 94.75%, respectively, while ZnO has almost

no photocatalytic properties. The improved photocatalytic activity of the composite is due to the synergistic effect of ZnO and g-C_3N_4. The connection of two semiconductors (ZnO and g-C_3N_4) will form a heterojunction at the contact surface. And the formed heterojunctions are beneficial to the effective separation of charge carriers. The presence of g-C_3N_4 in the ZCN sample overcomes the disadvantage of photogenerated electron-hole recombination that occurs in individual semiconductor materials.

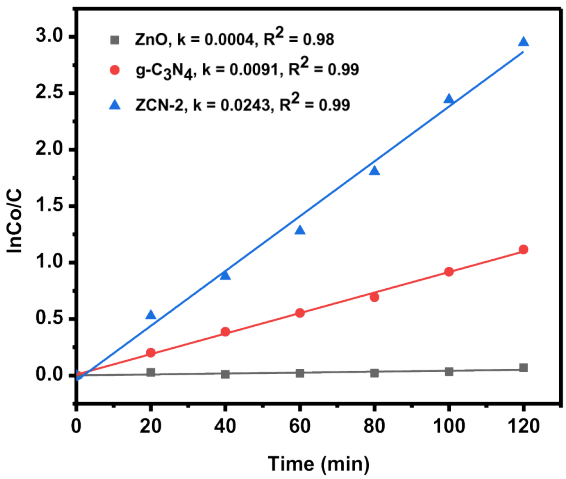

Figure 6. Plot of Langmuir-Hinshelwood model of ZnO, g-C_3N_4, and ZCN materials.

To investigate the kinetics of photocatalytic reactions, the Langmuir–Hinshelwood model is usually employed (Figure 6). It can be observed that the plots of ln(C_0/C) versus reaction time (t) are well fit by the pseudo-first-order rate model with high correlation coefficients R^2 (0.99–1).

The results show that the ZCN catalyst has the highest reaction rate (0.0243 min^{-1}), which is 2.76 times higher than g-C_3N_4, and is much more significant than ZnO material. This result indicates that adding g-C_3N_4 to ZnO significantly improved the photocatalytic activity of pure ZnO.

4. CONCLUSION

ZCN material is synthesized by a simple calcination method. This heterostructure shows the ability to effectively capture and store charge in the visible light region, significantly improving the photocatalytic efficiency of the material in the decomposition of RhB in a water environment. The reaction follows a Langmuir-Hinshelwood model with a calculated rate constant of 0.0243 min^{-1}. The ZCN composite material exhibits good heterojunction between ZnO and g-C_3N_4 and is a promising semiconductor material for decomposing organic dyes in water solution by photocatalysis under visible light.

REFERENCES

1. S. Ahmed, M. Rasul, R. Brown, M. Hashib. Influence of parameters on the heterogeneous photocatalytic degradation of pesticides and phenolic contaminants in wastewater: a short review, *Journal of Environmental Management*, **2011**, *92*(3), 311-330.

2. M. Azarang, A. Shuhaimi, R. Yousefi, S. P. Jahromi. One-pot sol–gel synthesis of reduced graphene oxide uniformly decorated zinc oxide nanoparticles in starch environment for highly efficient photodegradation of methylene blue, *RSC Advances,* **2015**, *5*(28), 21888-21896.

3. S. M. Jilani, P. Banerji. Graphene oxide–zinc oxide nanocomposite as channel layer for field effect transistors: effect of ZnO loading on field effect transport, *ACS Applied Materials & Interfaces,* **2014**, *6*(19), 16941-16948.

4. M. Azarang, A. Shuhaimi, R. Yousefi, A. M. Golsheikh, M. Sookhakian. Synthesis and characterization of ZnO NPs/reduced graphene oxide nanocomposite prepared in gelatin medium as highly efficient photo-degradation of MB, *Ceramics International*, **2014**, *40*(7), 10217-10221.

5. X. Huang, C. Tay, Z. Zhan, C. Zhang, L. Zheng, T. Venkatesan, S. Chua. Universal photoluminescence evolution of solution-grown ZnO nanorods with annealing: important role of hydrogen donor, *CrystEngComm,* **2011**, *13*(23), 7032-7036.

6. M. H. Suhag, A. Khatun, I. Tateishi, M. Furukawa, H. Katsumata, S. Kaneco. One-step fabrication of the ZnO/g-C_3N_4 composite for visible light-responsive photocatalytic

https://doi.org/10.52111/qnjs.2024.18304

degradation of bisphenol E in aqueous solution, *ACS Omega,* **2023**, *8*(13), 11824-11836.

7. S. Stolbov, S. Zuluaga. Sulfur doping effects on the electronic and geometric structures of graphitic carbon nitride photocatalyst: insights from first principles, *Journal of Physics: Condensed Matter*, **2013**, *25*(8), 085507.

8. M. Tahir, C. Cao, F. K. Butt, S. Butt, F. Idrees, Z. Ali, I. Aslam, M. Tanveer, A. Mahmood, N. Mahmood. Large scale production of novel gC_3N_4 micro strings with high surface area and versatile photodegradation ability, *CrystEngComm*, **2014**, *16*(9), 1825-1830.

9. B. Zhu, P. Xia, Y. Li, W. Ho, J. Yu. Fabrication and photocatalytic activity enhanced mechanism of direct Z-scheme g-C_3N_4/Ag_2WO_4 photocatalyst, *Applied Surface Science,* **2017**, *391*, 175-183.

10. X. Li, M. Li, J. Yang, X. Li, T. Hu, J. Wang, Y. Sui, X. Wu, L. Kong. Synergistic effect of efficient adsorption g-C_3N_4/ZnO composite for photocatalytic property, *Journal of Physics and Chemistry of Solids*, **2014**, *75*(3), 441-446.

11. K. Dulta, G. K. Ağçeli, P. Chauhan, R. Jasrotia, P. Chauhan. Ecofriendly synthesis of zinc oxide nanoparticles by Carica papaya leaf extract and their applications, *Journal of Cluster Science,* **2021**, 1-15.

12. B. V. Lotsch, M. Döblinger, J. Sehnert, L. Seyfarth, J. Senker, O. Oeckler, W. Schnick. Unmasking melon by a complementary approach employing electron diffraction, solid-state NMR spectroscopy, and theoretical calculations-structural characterization of a carbon nitride polymer, *Chemistry-A European Journal*, **2007**, *13*(17), 4969-4980.

13. J. Liu, T. Zhang, Z. Wang, G. Dawson, W. Chen. Simple pyrolysis of urea into graphitic carbon nitride with recyclable adsorption and photocatalytic activity, *Journal of Materials Chemistry*, **2011**, *21*(38), 14398-14401.

14. N. Nie, L. Zhang, J. Fu, B. Cheng, J. Yu. Self-assembled hierarchical direct Z-scheme g-C_3N_4/ZnO microspheres with enhanced photocatalytic CO_2 reduction performance, *Applied Surface Science*, **2018**, *441*, 12-22.

15. C. Xing, Z. Wu, D. Jiang, M. Chen. Hydrothermal synthesis of In_2S_3/g-C_3N_4 heterojunctions with enhanced photocatalytic activity, *Journal of Colloid and Interface Science*, **2014**, *433*, 9-15.

16. D. Jiang, L. Chen, J. Zhu, M. Chen, W. Shi, J. Xie. Novel p–n heterojunction photocatalyst constructed by porous graphite-like C_3N_4 and nanostructured BiOI: facile synthesis and enhanced photocatalytic activity, *Dalton Transactions*, **2013**, *42*(44), 15726-15734.

17. J. Hong, X. Xia, Y. Wang, R. Xu. Mesoporous carbon nitride with in situ sulfur doping for enhanced photocatalytic hydrogen evolution from water under visible light, *Journal of Materials Chemistry*, **2012**, *22*(30), 15006-15012.

18. D. R. Paul, S. Gautam, P. Panchal, S. P. Nehra, P. Choudhary, A. Sharma. ZnO-modified g-C_3N_4: a potential photocatalyst for environmental application, *ACS Omega*, **2020**, *5*(8), 3828-3838.

TẠP CHÍ KHOA HỌC
TRƯỜNG ĐẠI HỌC QUY NHƠN

Dạng tích phân cho một số mở rộng của bất đẳng thức Aczél

Lâm Thị Thanh Tâm*

Khoa Toán và Thống kê, Trường Đại học Quy Nhơn, Việt Nam

Ngày nhận bài: 23/01/2024; Ngày sửa bài: 01/03/2024
Ngày nhận đăng: 04/03/2024; Ngày xuất bản: 28/06/2024

TÓM TẮT

Bất đẳng thức Aczél xuất hiện lần đầu tiên vào năm 1956. Kể từ đó, nó đã thu hút sự quan tâm của nhiều nhà toán học. Từ đó các kết quả mở rộng và ứng dụng của bất đẳng thức này đã được công bố. Trong bài báo này, chúng tôi trình bày các phiên bản tích phân cho một số mở rộng của bất đẳng thức Aczél. Qua đó, chúng tôi thu được dạng tích phân cho các bất đẳng thức Aczél và Bellman.

Từ khóa: *Bất đẳng thức dạng Aczél, bất đẳng thức Popoviciu, bất đẳng thức Bellman.*

**Tác giả liên hệ chính.*
Email: lamthithanhtam@qnu.edu.vn

https://doi.org/10.52111/qnjs.2024.18305

QUY NHON UNIVERSITY
JOURNAL OF SCIENCE

Integral versions of some generalizations of Aczél's inequality

Lam Thi Thanh Tam*

Faculty of Mathematics and Statistics, Quy Nhon University, Vietnam

Received: 23/01/2024; Revised: 01/03/2024
Accepted: 04/03/2024; Published: 28/06/2024

ABSTRACT

Aczél inequality was first proposed in 1956. Then it has been considered by many mathematicians. Thus its generalizations and applications were published. In this paper we establish integral versions of some generalizations of Aczél's inequality. As a consequence, we obtain integral types of Aczél's inequality and Bellman's inequality.

Keywords: *Aczél-type inequality, Bellman's inequality, Popoviciu's inequality.*

1. INTRODUCTION

In 1956, a famous result of J. Aczél was published in the research[1] stated as follows.

Theorem A ([1]). *If* $a_1,\ a_2,\ldots,a_n,\ b_1,\ b_2,\ldots,b_n$ *are positive real numbers such that* $a_1^2 > a_2^2 + a_3^2 + \cdots + a_n^2$ *and* $b_1^2 > b_2^2 + b_3^2 + \cdots + b_n^2$, *then*

$$\left(a_1^2 - \sum_{i=2}^{n} a_i^2\right)\left(b_1^2 - \sum_{i=2}^{n} b_i^2\right) \leqslant \left(a_1 b_1 - \sum_{i=2}^{n} a_i b_i\right)^2. \tag{1}$$

Inequality (1) was later called 'Aczél's inequality'. In 1959, the first extension of (1) was provided by Popoviciu[3] and later called 'Popoviciu's inequality' stated as follows.

Theorem B ([3]). *Let* $p,\ q$ *be positive real numbers such that* $\dfrac{1}{p} + \dfrac{1}{q} = 1$ *and let* $a_1,\ldots,a_n,\ b_1,\ldots,b_n$ *be positive real numbers such that* $a_1^p > a_2^p + \cdots + a_n^p$ *and* $b_1^q > b_2^q + \cdots + b_n^q$. *Then*

$$\left(a_1^p - \sum_{i=2}^{n} a_i^p\right)^{1/p}\left(b_1^q - \sum_{i=2}^{n} b_i^q\right)^{1/q} \leqslant a_1 b_1 - \sum_{i=2}^{n} a_i b_i. \tag{2}$$

The next result is the famous Bellman's inequality. Although this inequality was discovered in 1934 by Hardy et al.[2], it is also considered as a Aczél-type inequality. Let us recall this inequality.

Theorem C ([2]). *Let* $a_1,\ldots,a_n,\ b_1,\ldots,b_n$ *be positive real numbers and* $p > 1$. *If* $a_1^p > a_2^p + \cdots + a_n^p$ *and* $b_1^p > b_2^p + \cdots + b_n^p$, *then*

$$\left(a_1^p - \sum_{i=2}^{n} a_i^p\right)^{1/p} + \left(b_1^p - \sum_{i=2}^{n} b_i^p\right)^{1/p} \leqslant \left[(a_1+b_1)^p - \sum_{i=2}^{n}(a_i+b_i)^p\right]^{1/p}. \tag{3}$$

*Corresponding author.
Email: lamthithanhtam@qnu.edu.vn

https://doi.org/10.52111/qnjs.2024.18305

Recently, some generalizations of inequalities (2) and (3) are presented by Chang-Jian Zhao and Wing-Sum Cheung.[4] These results are stated as the following theorems.

Theorem D ([4]). *Let p, q be positive real numbers such that $\frac{1}{p}+\frac{1}{q}=1$ and let a_i, b_i, a_{ji}, b_{ji} $(i=1,\dots,n, j=1,\dots,m)$ be positive real numbers such that*

$$\left(a_1^p-\sum_{i=2}^{n}a_i^p\right)-\left(\sum_{j=1}^{m}a_{j1}^p-\sum_{j=1}^{m}\sum_{i=2}^{n}a_{ji}^p\right)>0,$$

$$\left(b_1^q-\sum_{i=2}^{n}b_i^q\right)-\left(\sum_{j=1}^{m}b_{j1}^q-\sum_{j=1}^{m}\sum_{i=2}^{n}b_{ji}^q\right)>0,$$

$$\frac{a_{j1}}{b_{j1}}=\cdots=\frac{a_{jn}}{b_{jn}},\qquad j=1,\dots,m.$$

Then

$$\left(a_1b_1-\sum_{i=2}^{n}a_ib_i\right)-\left(\sum_{j=1}^{m}a_{j1}b_{j1}-\sum_{j=1}^{m}\sum_{i=2}^{n}a_{ji}b_{ji}\right)$$
$$\geqslant\left[\left(a_1^p-\sum_{i=2}^{n}a_i^p\right)-\left(\sum_{j=1}^{m}a_{j1}^p-\sum_{j=1}^{m}\sum_{i=2}^{n}a_{ji}^p\right)\right]^{1/p}$$
$$\times\left[\left(b_1^q-\sum_{i=2}^{n}b_i^q\right)-\left(\sum_{j=1}^{m}b_{j1}^q-\sum_{j=1}^{m}\sum_{i=2}^{n}b_{ji}^q\right)\right]^{1/q}. \tag{4}$$

Theorem E ([4]). *Let $p\geqslant 1$, a_i, b_i, a_{ji}, b_{ji} $(j=1,\dots,m, i=1,\dots,n)$ be positive real numbers such that*

$$\left(a_1^p-\sum_{i=2}^{n}a_i^p\right)-\left(\sum_{j=1}^{m}a_{j1}^p-\sum_{j=1}^{m}\sum_{i=2}^{n}a_{ji}^p\right)>0,$$

$$\left(b_1^p-\sum_{i=2}^{n}b_i^p\right)-\left(\sum_{j=1}^{m}b_{j1}^p-\sum_{j=1}^{m}\sum_{i=2}^{n}b_{ji}^p\right)>0,$$

$$\frac{a_{j1}}{b_{j1}}=\frac{a_{j2}}{b_{j2}}=\cdots=\frac{a_{jn}}{b_{jn}},\qquad j=1,2,\dots,m.$$

Then

$$\left[\left((a_1+b_1)^p-\sum_{i=2}^{n}(a_i+b_i)^p\right)-\left(\sum_{j=1}^{m}(a_{j1}+b_{j1})^p-\sum_{j=1}^{m}\sum_{i=2}^{n}(a_{ji}+b_{ji})^p\right)\right]^{1/p}$$
$$\geqslant\left[\left(a_1^p-\sum_{i=2}^{n}a_i^p\right)-\left(\sum_{j=1}^{m}a_{j1}^p-\sum_{j=1}^{m}\sum_{i=2}^{n}a_{ji}^p\right)\right]^{1/p}$$
$$\times\left[\left(b_1^p-\sum_{i=2}^{n}b_i^p\right)-\left(\sum_{j=1}^{m}b_{j1}^p-\sum_{j=1}^{m}\sum_{i=2}^{n}b_{ji}^p\right)\right]^{1/p}. \tag{5}$$

In the present paper we establish integral versions for inequalities (4) and (5). As a result, respective integral versions of inequalities (1) and (3) are obtained.

2. MAIN RESULTS

We first establish an integral version of inequality (4) in Theorem D as follows.

Theorem 2.1. *Let A, B, A_j, B_j $(j=1,\dots,m)$ be positive real numbers. Let f, g, f_j, g_j $(j=1,\dots,m)$ be positive Riemann integrable functions on $[a,b]$ such that*

$$U_2-U_{2,m}>0, \tag{6}$$

$$V_2-V_{2,m}>0, \tag{7}$$

$$\frac{f_j(x)}{g_j(x)}=\frac{A_j}{B_j},\qquad \forall x\in[a,b],\ j=1,2,\dots,m, \tag{8}$$

where

$$U_2=A^2-\int_a^b f^2(x)dx,$$

$$V_2=B^2-\int_a^b g^2(x)dx,$$

$$U_{2,m}=\sum_{j=1}^{m}A_j^2-\sum_{j=1}^{m}\int_a^b f_j^2(x)dx,$$

$$V_{2,m}=\sum_{j=1}^{m}B_j^2-\sum_{j=1}^{m}\int_a^b g_j^2(x)dx.$$

Then

$$[W_2 - W_{2,m}]^2 \geqslant [U_2 - U_{2,m}] \times [V_2 - V_{2,m}], \quad (9)$$

where

$$W_2 = AB - \int_a^b f(x)g(x)dx,$$

$$W_{2,m} = \sum_{j=1}^{m} A_j B_j - \sum_{j=1}^{m} \int_a^b f_j(x)g_j(x)dx.$$

Proof. For any positive integer n, we choose an equidistant partition of $[a, b]$ by $n+1$ points

$$x_0 < x_1 < \cdots < x_n,$$

with $x_0 = a$, $x_i = a + i\,\dfrac{b-a}{n}$, $\Delta x = x_i - x_{i-1} = \dfrac{b-a}{n}$, $i = 1, 2, \ldots, n$. Due to (6) and (7), it follows that there exists a positive integer number N such that for all $n > N$ we have

$$\left(A^2 - \sum_{i=1}^{n} f^2(x_{i-1})\Delta x\right) - \left(\sum_{j=1}^{m} a_j^2 - \sum_{j=1}^{m}\sum_{i=1}^{n} f_j^2(x_{i-1})\Delta x\right) > 0,$$

and

$$\left(B^2 - \sum_{i=1}^{n} g^2(x_{i-1})\Delta x\right) - \left(\sum_{j=1}^{m} b_j^2 - \sum_{j=1}^{m}\sum_{i=1}^{n} g_j^2(x_{i-1})\Delta x\right) > 0.$$

It follows from (8) that

$$\frac{f_j\left(a + (i-1)\dfrac{b-a}{n}\right)\left(\dfrac{b-a}{n}\right)^{1/2}}{g_j\left(a + (i-1)\dfrac{b-a}{n}\right)\left(\dfrac{b-a}{n}\right)^{1/2}} = \frac{A_j}{B_j},$$

for $j = 1, 2, \ldots, m$ and $i = 2, 3 \ldots, n$. Applying Theorem D with

$$p = q = \frac{1}{2},\ a_1 = A,\ b_1 = B,\ a_{j1} = A_j,\ b_{j1} = B_j,$$

$$a_i = f\left(a + (i-1)\frac{b-a}{n}\right)\left(\frac{b-a}{n}\right)^{1/2},$$

$$b_i = g\left(a + (i-1)\frac{b-a}{n}\right)\left(\frac{b-a}{n}\right)^{1/2},$$

$$a_{ji} = f_j\left(a + (i-1)\frac{b-a}{n}\right)\left(\frac{b-a}{n}\right)^{1/2},$$

$$b_{ji} = g_j\left(a + (i-1)\frac{b-a}{n}\right)\left(\frac{b-a}{n}\right)^{1/2}$$

for $j = 1, \ldots, m,\ i = 1, \ldots, n$, we obtain

$$\left(AB - \sum_{i=1}^{n} f(x_{i-1})\, g(x_{i-1})\, (\Delta x)^{\frac{1}{2}+\frac{1}{2}}\right) - \left(\sum_{j=1}^{m} A_j B_j - \sum_{j=1}^{m}\sum_{i=1}^{n} f_j(x_{i-1})\, g_j(x_{i-1})\, (\Delta x)^{\frac{1}{2}+\frac{1}{2}}\right)$$

$$\geqslant \left[\left(A^2 - \sum_{i=1}^{n} f^2(x_{i-1})\Delta x\right) - \left(\sum_{j=1}^{m} A_j^2 - \sum_{j=1}^{m}\sum_{i=1}^{n} f_j^2(x_{i-1})\Delta x\right)\right]^{1/2}$$

$$\times \left[\left(B^2 - \sum_{i=1}^{n} g^2(x_{i-1})\Delta x\right) - \left(\sum_{j=1}^{m} B_j^2 - \sum_{j=1}^{m}\sum_{i=1}^{n} g_j^2(x_{i-1})\Delta x\right)\right]^{1/2}.$$

Hence

$$\left(AB - \sum_{i=1}^{n} f(x_{i-1})\, g(x_{i-1})\,\Delta x -\right) - \left(\sum_{j=1}^{m} A_j B_j - \sum_{j=1}^{m}\sum_{i=1}^{n} f_j(x_{i-1})\, g_j(x_{i-1})\,\Delta x\right)$$

$$\geqslant \left[\left(A^2 - \sum_{i=1}^{n} f^2(x_{i-1})\Delta x\right) - \left(\sum_{j=1}^{m} A_j^2 - \sum_{j=1}^{m}\sum_{i=1}^{n} f_j^2(x_{i-1})\Delta x\right)\right]^{1/2} \times$$

$$\times \left[\left(B^2 - \sum_{i=1}^{n} g^2(x_{i-1})\Delta x\right) - \left(\sum_{j=1}^{m} B_j^2 - \sum_{j=1}^{m}\sum_{i=1}^{n} g_j^2(x_{i-1})\Delta x\right)\right]^{1/2}. \quad (*)$$

https://doi.org/10.52111/qnjs.2024.18305

Since $f,\ g,\ f_j,\ g_j$ are Riemann integrable on $[a,b]$, so are $f^2,\ g^2,\ fg,\ f_j^2,\ g_j^2$, and $f_jg_j\ (j=1,\ldots,m)$. Letting $n\to\infty$ in both sides of (*), we obtain (9). The proof is complete. □

In the case of $m=1$, we get an integral type of Aczél's inequality (1):

Corollary 2.2. *Let $A>0$, $B>0$, and let $f,g:[a,b]\to(0,\infty)$ be Riemann integrable functions such that $A^2>\int_a^b f^2(x)dx$ and $B^2>\int_a^b g^2(x)dx$. Then*

$$\left(A^2-\int_a^b f^2(x)dx\right)\left(B^2-\int_a^b g^2(x)dx\right)\leqslant\left(AB-\int_a^b f(x)g(x)dx\right)^2. \quad (10)$$

By using a similar method in the proof of Theorem 2.1, we get the following result, which is an integral version of inequality (5).

Theorem 2.3. *Let $p>1$, $A>0$, $B>0$. Let $a_j,b_j,\ (j=1,\ldots,m)$ be positive real numbers. Let $f,\ g,\ f_j,g_j\ (j=1,\ldots,m)$ be positive Riemann integrable functions on $[a,b]$ such that*

$$U_p-U_{p,m}>0, \quad (11)$$

$$V_p-V_{p,m}>0, \quad (12)$$

$$\frac{f_j(x)}{g_j(x)}=\frac{a_j}{b_j},\qquad x\in[a,b],\ j=1,2,\ldots,m, \quad (13)$$

where

$$U_p=A^p-\int_a^b f^p(x)dx,$$

$$V_p=B^p-\int_a^b g^p(x)dx,$$

$$U_{p,m}=\sum_{j=1}^m A_j^p-\sum_{j=1}^m\int_a^b f_j^p(x)dx,$$

$$V_{p,m}=\sum_{j=1}^m B_j^p-\sum_{j=1}^m\int_a^b g_j^p(x)dx.$$

Then

$$\left[H_p-H_{p,m}\right]^{1/p}\geqslant\left[U_p-U_{p,m}\right]^{1/p}+\left[V_p-V_{p,m}\right]^{1/p}, \quad (14)$$

where

$$H_p=(A+B)^p-\int_a^b\left[f(x)+g(x)\right]^p dx,$$

$$H_{p,m}=\sum_{j=1}^m(a_j+b_j)^p-\sum_{j=1}^m\int_a^b\left[f_j(x)+g_j(x)\right]^p dx.$$

Proof. For any positive integer n, we choose an equidistant partition of $[a,b]$ by $n+1$ points

$$x_0<x_1<\cdots<x_n,$$

with $x_0=a$, $x_i=a+i\ \dfrac{b-a}{n}$, $\Delta x=x_i-x_{i-1}=\dfrac{b-a}{n}$, $i=1,2,\ldots,n$. Owing to (11) and (12), there exists a positive integer number N such that for all $n>N$

$$\left(A^p-\sum_{i=1}^n f^p\left(x_{i-1}\right)\Delta x\right)-\left(\sum_{j=1}^m a_j^p-\sum_{j=1}^m\sum_{i=1}^n f_j^p\left(x_{i-1}\right)\Delta x\right)>0,$$

and

$$\left(B^p-\sum_{i=1}^n g^p\left(x_{i-1}\right)\Delta x\right)-\left(\sum_{j=1}^m b_j^p-\sum_{j=1}^m\sum_{i=1}^n g_j^p\left(x_{i-1}\right)\Delta x\right)>0.$$

Since (13) , it follows that

$$\frac{f_j(x_i)\left(\Delta x\right)^{1/p}}{g_j(x_i)\left(\Delta x\right)^{1/p}}=\frac{A_j}{B_j},\ j=1,2,\ldots,m.$$

Applying Theorem E with $a_1=A$, $b_1=B$, and for $j=1,\ldots,m,\ i=1,\ldots,n$

$$a_{j1} = A_j, \qquad b_{j1} = B_j,$$
$$a_i = f(x_{i-1})(\Delta x)^{1/p},$$
$$b_i = g(x_{i-1})(\Delta x)^{1/p},$$
$$a_{ji} = f_j(x_{i-1})(\Delta x)^{1/p},$$
$$b_{ji} = g_j(x_{i-1})(\Delta x)^{1/p}$$

we get

$$\begin{aligned}
&\left\{\left((A+B)^p - \sum_{i=1}^{n}\left[f(x_{i-1}) + g(x_{i-1})\right]^p \Delta x\right) - \right.\\
&- \left(\sum_{j=1}^{m}(A_j+B_j)^p - \right.\\
&\qquad \left.\left. - \sum_{j=1}^{m}\sum_{i=1}^{n}\left[f_j(x_{i-1}) + g_j(x_{i-1})\right]^p \Delta x\right)\right\}^{1/p}\\
&\geqslant \left[\left(A^p - \sum_{i=1}^{n} f^p(x_{i-1})\Delta x\right) - \right.\\
&\qquad \left. - \left(\sum_{j=1}^{m} A_j^p - \sum_{j=1}^{m}\sum_{i=1}^{n} f_j^p(x_{i-1})\Delta x\right)\right]^{1/p}\\
&+ \left[\left(B^p - \sum_{i=1}^{n} g^p(x_{i-1})\Delta x\right) - \right.\\
&\qquad \left. - \left(\sum_{j=1}^{m} B_j^p - \sum_{j=1}^{m}\sum_{i=1}^{n} g_j^p(x_{i-1})\Delta x\right)\right]^{1/p}.
\end{aligned} \tag{**}$$

Since $f,\ g, f_j, g_j$ are Riemann integrable on $[a,b]$, it follows that f^p, g^q, $(f+g)^p$, f_j^p, g_j^q, $(f_j+g_j)^p$, $j=1,\ldots,m$ are also Riemann integrable on $[a,b]$. Letting $n \to \infty$ in both sides of (**), we obtain (14). The proof of Theorem 2.3 is complete. □

By setting $m=1$ in (14), we obtain an integral version of the famous Bellman's integral as follows.

Corollary 2.4. *Let $p>1$, $A>0$, $B>0$. Let f and g be positive Riemann integrable functions on $[a,b]$ such that $A^p > \int_a^b f^p(x)dx$ and $B^p > \int_a^b g^p(x)dx$. Then*

$$\begin{aligned}
&\left(A^p - \int_a^b f^p(x)dx\right)^{1/p} + \left(B^p - \int_a^b g^p(x)dx\right)^{1/p}\\
&\qquad \leqslant \left((A+B)^p - \int_a^b \left[f(x)+g(x)\right]^p dx\right)^{1/p}.
\end{aligned} \tag{15}$$

Acknowledgment

This study is conducted within the framework of science and technology projects at institutional level of Quy Nhon University under the project code T2022.746.02.

REFERENCES

1. J. Aczél. Some general methods in the theory of functional equation in one variable, new applications of functional equations, *Uspekhi Mathematicheskikh Nauk*, **1956**, *11*(3), 3–68 (in Russian).
2. G. H. Hardy, J. E. Littlewwood, G. Pólya. *Inequalities*, Cambridge University of Press, Cambridge, 1934.
3. T. Popoviciu. On an inequality, *Gazeta Matematică si Fizică Seria A*, **1959**, *11*(64), 451–461 (in Romanian).
4. C. J. Zhao, W. S. Cheung. Generalizations of Popoviciu's and Bellman's inequalities, *Bulluten of Brazilian Mathematical Society, New series*, **2020**, *51*, 417–428.

https://doi.org/10.52111/qnjs.2024.18305